2008

Analytical solution to the wave equation with discrete pressure sources: A model for the Rijke tube

Eduardo G. Perez
West Virginia University

Analytical Solution to the Wave Equation with Discrete Pressure Sources: A Model for the Rijke Tube

Eduardo G. Pérez

Dissertation Submitted to the
College of Engineering and Mineral Resources
at West Virginia University
in partial fulfillment of the requirements
for the degree of

Doctor of Philosophy
in

Mechanical Engineering

Mridul Gautam, Ph.D., chair
Donald Ferguson, Ph.D.
John Loth, Ph.D.
Gary Morris, Ph.D.
George Richards, PhD.

Department of Mechanical and Aerospace Engineering

Morgantown, West Virginia
2008

Keywords: wave equation, discrete pressure sources, combustion instabilities

Abstract

Analytical Solution to the Wave Equation with Discrete Pressure Sources: A Model for the Rijke Tube

Eduardo G. Perez

Despite of having been studied for several decades the phenomena of combustion instabilities are not well understood. Pressure waves due to the combustion instabilities can become violent being detrimental for both the performance and combustor life. A good prediction of the pressure distribution inside the combustor is important in order to prevent the occurrence of this phenomenon. In this work a technique for solving the wave equation with discrete sources (or sinks) using the Green's functions was developed. One and two-dimensional approaches for cylindrical and Cartesian coordinates with constant speed of sound were solved. Also the case of one-dimensional axially varying temperature is presented. This technique was validated with results found in the literature and experimental data showing excellent agreement. By combining the 2-D solution with constant speed of sound plus the 1-D with axially varying speed of sound this technique accounts for the contributions of the fuel composition since the different blends of fuel produce different temperature profiles and therefore different speeds of sound. The technique is proposed to solve the 2-D pressure distribution of the Rijke tube, which can be considered as the simplest combustor configuration. The study of the pressure distribution in the Rijke tube is fundamental for the understanding of the phenomenon of combustion instabilities.

DEDICATION

To my son, to be born soon... my motivation already

ACKNOWLEDGMENT

Morgantown, where West Virginia University is located, is full of incredibly nice people that I would like to express my deepest thankfulness; people at WVU, the National Energy Technology Laboratory (NETL) and friends that I met while living in Morgantown.

In WVU I would like to express my gratitude to my advisor Dr. Gautam for his guidance, advice and support even after leaving Morgantown; to Dr. Prucz for his support and willingness to help. Also I would like to express my gratitude to the other members of my committee Dr. John Loth and Dr. Gary Morris. My special thanks to Dr. Barbero for not only making us feel as students but as family; his support, guidance and friendship were always there whenever I needed it.

In NETL I would like to thank Dr. Ferguson for being always supportive, for his friendship and academic advising. I would like to express my gratitude to Dr. Richards for being supportive and optimistic with my work. Also I would like to thank Douglas Straub M.S., Dr. Kent Caleston, Dr. Steven Woodruff and Dr. Daniel Maloni for giving me the opportunity to work my research at the Department of Energy - NETL.

I also would like to thank my friends and colleagues Omar Meza, Julio Noriega, Francisco "Fito" Pino, Francisco Elizalde, Alex Tsai, Herman Alcazar; and also to the Inter-American University of Puerto Rico specially to my friend Amilcar Rincon.

Finally I would like to thank my wife; her always unconditional love, support and encouraging words were very important for reaching this goal.

Table of Contents

List of Figures

List of Symbols

a, b, a_i, b_i	Arbitrary constants
c	speed of sound
F	Source (or sink) function
G or $G(\vec{x},\vec{x}')$	Green's Function
h and g	Initial conditions
H	Characteristic width
H(x-a)	Step function
J_ν	Bessel functions or order ν
k	Wave number
K	Kelvin degrees
L	Characteristic length
n	Integer positive number
p	Acoustic pressure
R	Gas constant
r	Radial distance
r_0	Characteristic radius
t	Time
T	Absolute temperature
$\vec{x}$	Field point
$\vec{x}'$	Source point
x and y	Cartesian coordinates

z	Axial distance
α	Source frequency
β	Argument of the Bessel function
γ	Specific heats ratio
$\delta(x-a)$	Dirac-Delta function
τ	Source time
ε	Very small number (ie. $\varepsilon \rightarrow 0$)
ν	Order of the Bessel functions
Λ	Strength of the source
θ	Angular displacement for cylindrical coordinates

CHAPTER I

INTRODUCTION

The collective name for NO and NO_2 is NOx (oxides of Nitrogen). Its major source of production in the atmosphere comes as a product of fossil fuel combustion. NOx emissions are known to contribute to several health related problems, such as aggravation of asthmatic conditions. In addition, NOx contribute to the production of tropospheric ozone and acid rain; hence there are environmental implications as well [1].

Continued concerns have lead to more restrictive regulations regarding NOx emissions from fossil fuel combustion, such those from gas turbine power generation systems. One means of complying with these demands is the use of the gas turbines operating under lean premixed (LP) combustion mode. As a consequence, the demand of this kind of system has recently increased.

Unfortunately, without downstream dilution and acoustic damping offered by diffusion flames, LP combustion is sensitive to small heat release and flow fluctuations that may result in unstable combustion. Unstable combustion is detrimental to both performance and combustor life. Several factors as combustion acoustics, flame stability, pollutant emissions and combustor efficiency are affected by unstable combustion. Although extensive research has been done on these topics, it is not very well understood. In order to prevent and control these instabilities, an appropriate understanding of the responsible mechanisms must be developed.

Thermo-acoustic instabilities are one of the major problems as pressure oscillations resulting from a number of sources can couple with heat release fluctuations causing violent vibrations directly affecting the combustor life and, as a consequence, the system performance and pollutant emissions. This leads to the added expense of shutting down the system for combustor maintenance and/or replacement.

Several studies have shown that combustors operating under LP combustion are sensitive to equivalence ratio fluctuations [2], [3], [4]. These fluctuations are convected downstream eventually producing large amplitude disturbances in the heat release if the proper conditions are given. The heat release drives the combustor pressure oscillations and the pressure and velocity oscillations drive the equivalence ratio fluctuations closing the feedback loop that maintains the instabilities. This coupling is referred to as the Rayleigh criterion which is shown schematically in figure 1.1.

A number of researchers devoted to study the problem of thermo-acoustic instabilities have reported an extensive amount of works that characterize the conditions and set the operational limits under which the instabilities occur [5],[6], [2]. Others are theoretical studies that have attempted to bring more insight to the mechanisms that drive the instabilities and to predict their occurrence [7], [8], [9]. Also, to a lesser degree, there are reports of CFD and computational models [10], [11], [12], [13]. All these works bring more understanding to this complex phenomenon. However, despite these efforts, there is a lack of complete agreement about the mechanisms responsible for the onset of combustion instabilities.

The main goal of this research is to predict the pressure distribution in a Rijke tube. The 2-D proposed model includes a 1-D axial temperature variation. This

temperature variation is expected to predict the effect of the fuel composition on the thermo-acoustic instabilities in the combustor since temperature profiles will depend on the fuel blend. Fuel composition, which affects both the chemistry and physics of the combustion process, might also affect the excitation of some instability mechanisms [1]

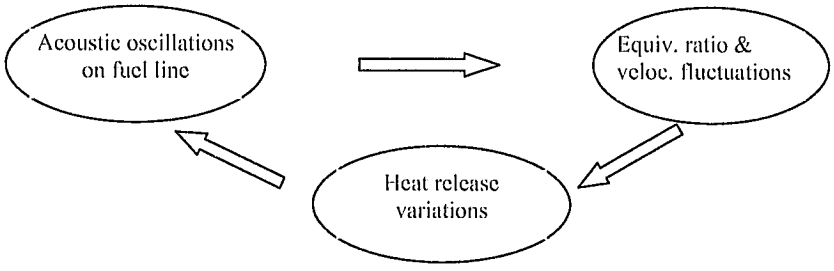

Fig.1.1. Schematic of thermo-acoustic instability feedback loop.

In the absence of guidance of a strict regulatory standard, the large number of domestic and international fuel suppliers has lead to variations in fuel compositions, and also heating values. For example, synthetic gas (syngas) fuels are typically composed of H_2 and CO, and may also contain smaller amounts of CH_4, N_2, CO_2, H_2O and other higher hydrocarbons. The fuel composition does not depend only on the site where the fuel has been originated from, but also on the processing technique. In addition, interest in utilizing other energy sources, fuel dependability and environmental concerns have motivated the use of biomass, landfill gas, or process gas. All these fuels can have widely differing properties.

The topic on fuel variability is currently under investigation but very few reports can be found in the literature. Some concerns about the effects of fuel variability on the combustion process have been raised but most of the works reported deal with hydrogen-

enriched fuels [14], [15], [16]. Some of these concerns include flashback and flame anchoring, autoignition, static and dynamic stability, and achieving emissions goals [17].

If the fuel composition is proven to be an important parameter in the excitation of combustion instabilities then this will have a great impact in several aspects such as regulations, combustor design and manufacturing. For combustors already in use new regulations and/or more strict fuel specifications will have to be issued in order to have systems that comply with the safety and emissions standards. For new equipment, design and manufacturing will have to be accommodated to allow a wide range of fuel compositions. Therefore, the economy of several industries could also be highly affected.

Studies reported by some researchers on the effects of fuel variability suggest that fuel composition has a significant impact on some parameters of the combustion process. Schefer [15] reported that the addition of up to 20% hydrogen to a methane/air mixture extended the lean stability limits of a swirl-stabilized flame. Natarajan et al. [14] reported that the flame speed of a $H_2/CO/CO_2$ mixture increased as the H_2 content and equivalence ratios increased. Similar results are reported by Zhang et al. [16].

The previous statements highlight the importance of having a model able to predict the effect of fuel composition on the thermo-acoustic instabilities in a combustion process. In order to achieve the main goal of this project a 2-D mathematical acoustic model that included a 1-D spatially variable temperature distribution was developed to predict how changes in fuel composition may alter the acoustic characteristics of a combustor under lean premixed conditions. Some basic cases were solved with this technique and the results were compared to those obtained from traditional theoretical

techniques, such as the Separation of Variables technique. Results were also compared to those obtained from experiments for a pipe with a side branch and an acoustic source.

The Rijke tube arrangement was employed to theoretically predict changes in the acoustic response as a result of varying temperature in the combustor. These varying temperatures can be related to the quantities of methane, ethane and propane in the fuel along with the equivalence ratio. For the acoustic part of the problem an analytical mathematical model was proposed that considered a 2-D spatial distribution (since no variation is expected with angular position) with constant speed of sound except where the flame and combustion gases are present. Where the flame and combustion gases are present the model considered an axially varying speed of sound. This feature is expected to account for the fuel compositions effects since the different blends of fuels have different heating values, which affect the heat release which in turn produces different gas temperatures. The speed of sound (c) is related to the temperature of the ideal gas by the relation $c = \sqrt{\gamma.R.T}$ where γ is the specific heats ratio, R is the gas constant and T is the temperature of the gas; therefore accounting for the temperature variation also implies accounting for the speed of sound variation.

The Green's functions were used as the main mathematical tool for the development of the analytical model. Green's functions have been proven to be powerful in other fields such as electrodynamics, fluid mechanics, heat transfer and others [18], [19], [20], [21], [22], [23]. There are few reports on the use of Green's functions in acoustics [24], but to the author's knowledge there are no reports on the use of discrete acoustic sources. This played a key role in the development of the mathematical model proposed in this work.

CHAPTER II

LITERATURE REVIEW

This chapter provides a review of some of the most representative works done in the topics of thermo-acoustic instabilities and fuel variability.

One of first reported works in thermo-acoustic instabilities may be tracked back to the ninetieth century when Higgins (1802) discovered what he called "singing flames" [12]. The sound produced when a jet of ignited gas was inserted into a tube open at both ends. The frequency of singing coincided with the natural frequency of the tube. Sound was produced only at certain ranges of system parameters. Years later, in 1859, Rijke made modifications to the Higgins experimental setup and reported what it is now known as the Rijke tube [25]. Rijke placed a heated wire screen in an open-ended vertical pipe. He noticed that strong oscillations occurred when the wire was placed in the bottom half of the pipe. When the heater was placed in the upper half, the oscillations were damped instead of driven. Rijke also reported that the oscillations stopped when the upper end of the pipe was sealed suggesting that the upward convective air currents were essential for the thermo-acoustic oscillations to take place.

The Rijke tube is the fundamental device used for the study of thermo-acoustic instabilities. The geometry of this device typically has a large length-to-diameter ratio and is much simpler than a full scale combustor of a gas turbine.

Rijke and several researchers of the ninetieth century expended a lot of time and effort trying to explain the phenomenon of thermo-acoustic instabilities. The success

came when Lord Rayleigh (in 1878) stated the fundamentals for the occurrence of this phenomenon. Lord Rayleigh's famous criterion states: "If heat be periodically communicated to, and abstracted from, a mass of air vibrating (for example) in a cylinder bounded by a piston, the effect produced will depend upon the phase of the vibration at which the transfer of heat takes place. If heat be given to the air at the moment of greatest condensation, or be taken from it at the moment of greatest rarefaction, the vibration is encouraged. On the other hand, if heat be given at the moment of greatest rarefaction, or abstracted at the moment of greatest condensation, the vibration is discouraged." Rayleigh Criterion establishes the basis for the occurrence of the thermo-acoustic instabilities but it does not provide sufficient detail to explain all of the characteristics of the thermo-acoustic instabilities response of a combustor.

In 1953 Putnam and Dennis [26] studied the oscillations in three different configurations. These configurations were: open-open tube with pre-mixed flame; closed-open tube with pre-mixed flame and, closed-open flame with diffusion flame. Their conclusion was that amplification of the oscillations occurs when two conditions were satisfied simultaneously: first, the difference between the rate of heat release and the pressure fluctuations was less than $\pi/4$; second: the point of heat release was close to a point of maximum pressure amplitude. They also demonstrated the validity of Rayleigh Criterion from the thermodynamic point of view. The authors presented a thermodynamic analysis in detail determining the phase requirements for the thermal oscillations to be driven. In 1954 the same authors [27] investigated the oscillations in a combustion chamber with a mesh-screen flame holder. In this research the gases were allow to pass through a converging nozzle and stack where the length of the stack and the depth of the

flame holder could be varied. Again, in 1956, Putnam and Dennis [28] conducted a survey on organ-pipe oscillations in combustion systems. Later, in 1971, Putnam [29] states the Rayleigh Criterion in an integral form and provides the condition for the combustion driven oscillations to occur. This condition was also expressed in integral form as a function of the acoustic pressure, the heat release and the angular frequency.

Blackshear [5], instead of examining the spontaneous excitation, in his experimental work analyzed the effect of a flame on a standing wave by measuring the ability of the flame to damp an imposed standing wave. In this paper the author explains the mechanism by which the heat addition can damp or drive an oscillation which basically reduces to satisfying the Rayleigh criterion.

By applying linear perturbation analysis to the conservation equations, Carrier [30], obtained a set of linearized partial differential equations describing oscillating properties in the cold and hot gases. Unlike Neuringer and Hudson [8], Carrier's 2-D analysis in cylindrical coordinates included the effects of viscosity at the tube walls. His solution, obtained by the separation of variables technique, for the fluctuating velocity potential was in the form:

$$\phi_j'(x,r,t) = \hat{\phi}_j(r)e^{i(\omega t - k_j x)}$$

where r is the radial coordinate, k is the wave number and ω the angular frequency.

In 1960, Crocco et al. [7] developed a time lag model (also referred as the n-τ model) for combustion instabilities in liquid-rocket engines. The model provided a way to couple heat perturbations with flow-field perturbations. This was achieved by a pressure-interaction index n, describing how the pressure oscillation affects combustion, and a time lag τ between the two fluctuations. The time lag was defined by Putnam [29]

as the interval between the time when the pressure disturbance occurs at the flame and the time when the heat is released at that location. Later, in 1969, Crocco and Mitchell [31] considered the time lag model but the oscillations were considered to be nonlinear.

Several researchers have published reviews in the area of thermo-acoustics and Rijke tubes along the years. Feldman [32] provided a short review of literature on thermo-acoustic oscillations in Rijke tubes and the previously mentioned survey by Putnam and Dennis [28]. Raun et al. [33] gave an extensive review of thermo-acoustic devices, especially Rijke tubes. They discussed the history, mechanisms of heat-driven acoustic instability, and experimental and analytical works on the Rijke tube. Oyediran et al. [24] presented a review on a variety of combustion devices focusing on theoretical and experimental investigations of unsteady heat release rate. The authors concluded that the boundary conditions had been well documented for rockets but more studies needed to be done for other combustion systems.

In 1987, Culik [8] presented a short communication on the Rayleigh criterion. In this work he was concerned with direct transfer of heat to the mechanical energy of acoustical motion. Culik provided an explicit formulation of the Rayleigh Criterion showing how it may be accommodated in a general analysis of pressure oscillations. The author started from a wave equation for the pressure fluctuation and an equation for the normal acoustic modes, which are the solution to the eigenvalue problem with Neumann boundary conditions: $\nabla^2\psi_n + k_n^2\psi_n = 0$. Culik combined these two equations, after using the Green's theorem and further simplifications he found an expression for the change of energy as a function of heat release fluctuation and pressure normal modes with time dependent amplitudes.

Dowling [6] used a simple geometry to determine the influence of several flow parameters on the frequency of the oscillations. With basic examples the author established that it has a critical effect the form of the coupling between the heat input and the unsteady flow in the frequency of the oscillations. Furthermore, Dowling used the same elementary examples to compare with the different methods found in the literature. The author concluded that those methods do not fully account for this effect. The cases considered for comparison were a homogeneous wave equation, the Green function technique reported by Hedge et al. [34], and finally the linearized Galerkin method employed by Culik [35]. In a posterior section of her paper, Dowling considered the effects of the mean flow, effects of drag, and the effects of distributed heat input. The author reported that mean flow effects in the thermo-acoustic oscillations can be important for Mach numbers as low as 0.15. For the drag force, she affirms that a flameholder with a blockage ratio of 25% or less has a negligible effect on the frequency of thermo-acoustic oscillations for inlet Mach numbers $0 \leq M \leq 0.15$. The author also reported that a distribution of the heat input over an axial distance (d) can lead to a significantly different frequency of oscillation from that when the heat input is concentrated.

Several mechanisms identified to contribute to acoustic instabilities have been investigated by researchers. Some of those mechanisms are the equivalence ratio, vortex shedding, entropy waves, and also purely chemical-kinetic considerations. Equivalence ratio has been studied by Lieuwen and others [2], [3]. They found that combustors operating under lean premixed mode of combustion are highly sensitive to variations in the equivalence ratio (Φ). They found that such equivalence ratio fluctuations can be

induced by interactions of the pressure and flow oscillations with the reactant supply rates. The authors reported that the perturbations formed at the inlet duct are convected by the mean flow to the combustor were they produce large amplitude heat release oscillations. They suggested that passive control approaches may not be viable means of controlling the combustions instabilities due to the multiple number of modes that may be excited by the combustion process. A measurement technique to determine the fluctuations in the equivalence ratio was developed by Mongia et al. [36]. Peracchio and Proscia [37] developed a one-dimensional model describing the linear acoustics with the non-linear heat release that accounts for the equivalence ratio oscillations. Richards and Robey [4] showed that the thermo-acoustic oscillations could be actively controlled by oscillating the fuel flow rate and hence the equivalence ratio between the two values which exhibit stable operation and thus effectively avoiding the equivalence ratio which is unstable. This process generates oscillations around a mean value of equivalence ratio that nullifies the oscillations produced by thermo-acoustic instabilities.

Vortex shed at the flame holder as a possible source of combustion instability was investigated by Poinsot et al. [38]. They reported that the instability is triggered when the vortices shed at the flame holder entrain unburned mixture, which propagates and causes a sudden change in heat release at some point downstream. This triggers an acoustic wave that propagates upstream closing the feedback loop. This mechanism is believed to be important in the distortion of the flame front by flow oscillations [39]. These flow oscillations can arise from either acoustic velocity oscillations that accompany the pressure perturbations, or from vortices that are carried with the flow. The flame can become wrapped up in these vortices so that its surface area and local rate of propagation

fluctuate in time. This latter mechanism has also been a major contributor to combustion oscillations in ramjets and afterburners [40]. A number of studies have been devoted to study the response of the flame to an acoustic disturbance.

An upstream acoustic wave is propagated when the hot spots present in a mean gas flow reach the inlet of a choked nozzle, causing acoustic instabilities; this phenomenon is known as entropy waves [41]. Effects of entropy waves had been assumed to exist at low frequencies [42].

A comprehensive review of these mechanisms has been done by Ibrahim et al. [41]. In this document they discussed extensively the mechanisms that contribute to combustion instabilities summarizing the theory used by previous researchers. In other section of this work they summarize the methods used to analyze and/or predict the onset of combustion instabilities. They also included a section to summarize the main parameters and studies done on the damping of the oscillatory combustion instabilities.

All works mentioned above give more insight to the phenomenon of combustion instabilities. For a given fuel, particular mechanisms that are believed to be responsible for the onset of the combustion instabilities were studied, however few reports on effects of fuel variability are found in the literature. Moliere [43] discussed the influence of fuels in gas turbines. In this work the author presented a qualitative description on what aspects of the combustion are expected to be affected. Based on a thermodynamic analysis Moliere discussed the influence of fuels on blow-off, flash-back, auto-ignition, characteristic reaction time, and deflagration-to-detonation transitions but no concerns on thermo-acoustic instabilities were addressed. Schefer [15] studied the stability characteristics of a pre-mixed, swirl-stabilized flame to determine the effects of hydrogen

addition. The author used OH planar laser-induced fluorescence (PLIF) to study the behavior of OH mole fraction as the lean stability limit was approached. In his experimental results the author reported a significant increase in the OH concentration and extended lean stability limits of the burner with the addition of up to 20% hydrogen to the methane/air mixture. A study on the influence of variations in the natural gas properties on the combustion process in terms of emissions and pulsations for a heavy-duty gas turbine was reported by Nord and Andersen [44]. The authors collected and analyzed data from a commercially operational gas turbine (ALSTOM GT11N1) concluding that normal day-to-day variations in the natural gas properties do no have a significant effect on the emissions and combustion instabilities; however, larger sudden changes could lead to considerable changes in the combustion behavior of the unit. Natarajan et al. [14] studied the effects of H2/CO/CO2 mixtures but they restricted their work to the laminar flame speed. In this study the authors measured the laminar flame speed over a range of fuel compositions, lean equivalence ratios, and reactant pre-heat temperatures. They reported that the flame speed increased as the H2 content of the fuel raised and for higher equivalence ratios. Similar conclusions were reported by Zhang et al. [16]. In this work the fuel consisted of H_2/CO/CH_4 mixtures. In a more recent work, Hendricks and Vandsburger [45] studied the response in heat release rate of the flame to acoustic perturbations of three gases: methane, ethane and propane which are the major components of natural gas. The authors concluded that changes in the fuel composition are tied to the thermo-acoustic stability of the system by affecting its flame dynamics.

It is seen that an accurate measurement of the heat release is an important task in studying thermo-acoustic oscillations. Unfortunately there is not a direct method of

measuring the heat release; instead indirect methods have to be used. For measurements of the heat release oscillation, OH* radiation is used. OH* are excited OH-radicals which, when going from their excited state to their ground state, emit light in the ultraviolet range, and assumed to be proportional to the heat release. Some researchers as Gaydon [46] and Diederichsen and Gould [47], have studied this phenomena giving more insight into this area.

The principle of particle image velocimetry (PIV) has been used in the scientific community to plot vector maps of instantaneous velocity fields. In most applications of PIV,"tracer particles have to be added to the flow. These particles have to be illuminated in a plane of the flow at least twice within a short time interval. The light scattered by the particles has to be recorded either on a single frame or on a sequence of frames. The displacement of the particles images between the light pulses has to be determined through evaluation of the PIV recordings" (Raffel [48]). An extensive explanation of this technique can be found in Ferguson [49]. In this work the author used time-resolved PIV to quantify the near-field acoustics and the dilatation rate field in the pre- and post-flame regions of the flow. In his experiments the author observed that multi-dimensional acoustics dominate the pre-combustion flow field with radial and axial acoustic velocities of similar magnitudes.

In summary, the use of the Green's functions has not been very extensive in the study of acoustics. There are in the literature very few analytical solutions for the wave equation using Green's functions, such those solved by Shao and Mechefske [50]. In their work the authors used the GF to find an approximation model to describe the sound radiation of magnetic resonance imaging (MRI) scanners. At difference to this work, they

did not considered acoustic sources in their model. In conduction heat transfer Venkataraman et al. [23] used the GF technique to find analytical solutions for the temperature distribution for thin circular plates and spheres with discrete heat sources. In this study the authors applied the GF technique with the method of images (also known as physical approach). The main restriction in this work was that their technique is only applicable for steady state cases, which is not applicable to the wave equation because of the oscillatory behavior of this phenomenon. In this work the GF was applied with a more classical approach using the expansion in infinite series obtained from separation of variables.

CHAPTER III

THEORETICAL BACKGROUND

3.1 THE GREEEN'S FUNCTION

It is known that analytically solving the wave equation with acoustic generating sources (i.e. non-homogeneous problem) can be complicated and challenging. Usually these kinds of problems have to be solved using numerical methods which in turn can produce inaccuracies, especially at points close to the acoustic source. Also, it is well known that hyperbolic equations (wave equation) are usually unstable when using finite difference methods. The problem becomes even more difficult if in addition to being non-homogeneous, a variable speed of sound is also considered. In this work, using a novel Green's functions technique, one and two dimensional solutions for the wave equation with discrete sources and various boundary conditions are proposed. Cartesian and cylindrical coordinates were considered. The one-dimensional case of variable speed of sound was also considered. These individual solutions were then added to build up the proposed model for the Rijke tube. Since Green's function is a cause-effect function, complex geometries can be solved by breaking them into more simple ones and adding their corresponding solutions. This characteristic of adding solutions is one of the advantages of the Green's Functions technique proposed in this work. In addition, a 3-D

problem of a pipe with a side branch in cylindrical coordinates is presented for validation purposes.

George Green first introduced Green's Function as early as 1828 in the essay entitled "On the Application of Mathematical Analysis to the Theories of Electricity and Magnetism" [51]. In this essay he derived the integral identities and used them to obtain integral representations for the solution of problems involving the Laplacian operator where $G(\vec{x},\vec{x}')$ is the effect at the field point $\vec{x}$ due to a unit source applied at the source point $\vec{x}'$.

Green's Functions are very powerful tools and have been used for many decades for obtaining solutions in electromagnetic theory, elasticity, fluid mechanics, and heat conduction, etc [18], [19], [20], [21], [22], [23]. However, their use in acoustics has not been very common especially among engineers. There are in the literature some analytical solutions for the wave equation using Green's functions such as those solved by Shao and Mechefske [50]. In this work the authors used the GF to find an approximation model to describe the sound radiation of magnetic resonance imaging (MRI) scanners. At difference to this work, they did not consider acoustic sources in their model.

The GF are expressions that depend on the geometry and the boundary conditions of the problem at hand. GF are found and presented later in this chapter.

3.2 THEORY REVIEW

For a better understanding of the development of the proposed model and the solutions for the particular cases, the Dirac-Delta and the Heavyside functions are briefly introduced as a necessary mathematical background. These functions are especially useful when mathematically expressing the sources.

3.2.1 Dirac-Delta function

Suppose that a vertical unit force is applied at a point resting on a plate, which extends along x-axis (with $-\infty<x<\infty$), as shown in Figure 3.1. The interest is in the force distribution F(x), in which function F is unknown but it can be asserted that it is concentrated (Figs. 3.1 and 3.2) in such a way that the net force is the unity. Therefore, F(x) must satisfy the following condition:

$$\int_{-\infty}^{\infty} F(x)dx = 1 \qquad (3.1)$$

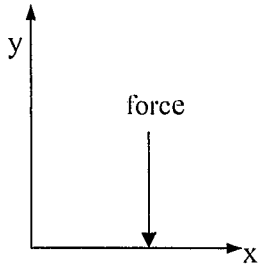

Figure 3.1 Applied force.

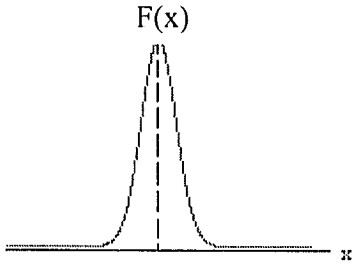

Figure 3.2 Force distribution.

Function F(x) is closely related to the notion of Dirac-Delta function. Here F represents not only the force in the example but a mass in gravitational field, a heat source in heat conduction, a charge in electrostatics or any other phenomena applied on a point. As said before, Green's Function is a cause-effect function where $G(\bar{x},\bar{x}')$ is the

effect at the field point $\bar{x}$ due to the unit source applied at the source point $\bar{x}'$. In this context it can be said that the Dirac-Delta function is also related to Green's function.

Consider a function as shown in figure 3.3

$$\left.\begin{array}{l} f(x) = \dfrac{1}{a} \quad \text{if} \quad -\dfrac{a}{2} < x < \dfrac{a}{2} \\ f(x) = 0 \quad \text{if} \quad x < -\dfrac{a}{2} \ \text{or} \ x > \dfrac{a}{2} \\ \text{Area of rectangle ABCD} = 1 \end{array}\right\} \quad \ldots. \quad (3.2)$$

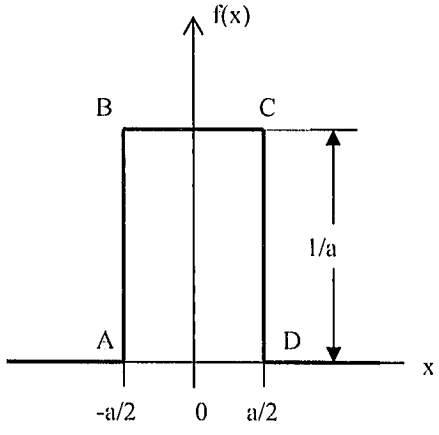

Figure 3.3 Intuitive idea of Dirac-Delta function.

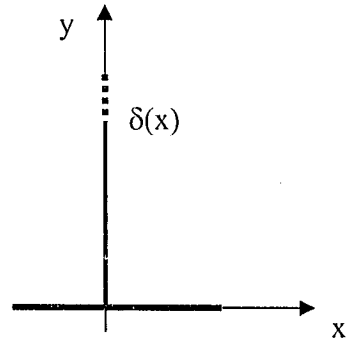

Figure 3.4 Dirac-Delta function.

Figures 3.3 and 3.4 together with the previous paragraphs give an intuitive idea of the Dirac-Delta function as "a" becomes smaller; f(x) tends to infinity in such a way that the area is constant and equal to the unity.

Dirac-Delta function δ(x) is a function defined such that it satisfies the following conditions:

$$\left.\begin{array}{l}\delta(x)=0 \quad \text{if} \quad x\neq 0\\ \delta(x)\to\infty \quad \text{if} \quad x=0\\ \int_{-\infty}^{\infty}\delta(x)dx=1\end{array}\right\}\ \text{Dirac-Delta function (special case)}$$

In general (see Figure 3.5):

$$\left.\begin{array}{l}\delta(x-a)=0 \quad \text{if} \quad x\neq a\\ \delta(x-a)\to\infty \quad \text{if} \quad x=a\\ \int_{-\infty}^{\infty}\delta(x-a)dx=1\end{array}\right\}\ \text{General form of Dirac-Delta function}$$

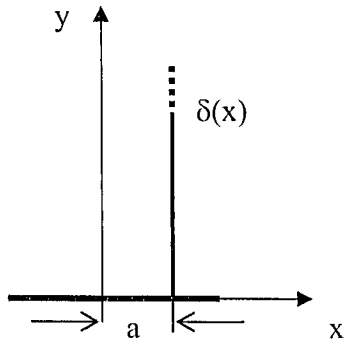

Fig. 3.5 Dirac-Delta Function, General Form

In addition to equation (3.2) Dirac-Delta conditions can be satisfied by several functions such as: $\delta(x)=\lim_{\sigma\to 0}\left[\frac{1}{\sqrt{4.\pi.\sigma}}.e^{\frac{-x^2}{4.\sigma^2}}\right]$

Some properties of Dirac-Delta function are used along the development of this work. These properties are the following:

1. $\int_{-\infty}^{\infty}\delta(x-a)dx=\int_{\alpha}^{\beta}\delta(x-a)dx=1 \qquad \alpha<a<\beta$

2. $\int_{a}^{b}f(x)\delta(x-\zeta)dx=f(\zeta) \qquad a<\zeta<b$

3. $\int_{b}^{c}f(x)\delta'(x-a)dx=-f'(a) \qquad b<a<c$

4. $\frac{\delta(x-a)}{(x-a)}=-\delta'(x-a)$

The primes in f and δ indicate first derivative.

Proofs of these properties are out of the scope of the present work, however proof of the second property which is used extensively in the development of the Green's Functions Solution Equation, can be found in appendix [A].

Dirac-Delta function can be extended to two and three-dimensional cases as well. For example three-dimensional Delta function is defined as:

$$\delta(\vec{x}-\vec{x}') = \delta(x-x')\delta(y-y')\delta(z-z')$$

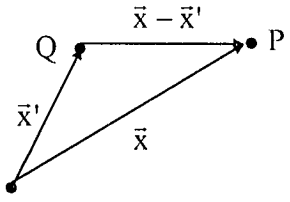

where:

point P location is represented by $\vec{x} = (x,y,z)$

point Q location is represented by $\vec{x}' = (x',y',z')$.

The properties remain the same as in the 1-D case:

$$\iiint_{v} \delta(\vec{x}-\vec{x}')d^3\vec{x}' = 1$$

$$\iiint_{v} f(\vec{x}')\delta(\vec{x}-\vec{x}')d^3\vec{x}' = f(\vec{x})$$

CHAPTER IV

MATHEMATICAL DEVELOPMENT

4.1 . THE PROPOSED MATHEMATICAL MODEL

The Green's Function Solution Equation (GFSE) and the Green's function itself played a major role in the development of the mathematical model presented in this study. For a given geometry the GFSE is unique and it is an integral expression in terms of the Green's function (represented by G in the equation) and the boundary conditions. After the GFSE was found the next step was to find G for the specified geometry and its particular boundary conditions. The final step was to express the source in a mathematical form and plug it into the GFSE. The source can be discrete or uniformly distributed along the geometry under study.

Green's functions technique has the advantage that complex geometries can be solved by breaking them into simple ones and adding the results. This advantage was used in this study for the proposed model of the Rijke tube combustor.

Figure 4.1a shows a schematic of the Rijke tube. This apparently simple geometry, in fact produces a complex pressure distribution when an acoustic source acts in the inner pipe. Classical analytical solutions fail for cases such as this. In fact, classical analytical solutions do not work for cases where discrete sources are considered. In this study the proposed model separates the Rijke tube in different regions as shown in figure

4.1b. Region I includes the inner pipe. A 2-D model with constant speed of sound was considered for this region however, results showed a 1-D behavior (i.e. no variation in the radial direction was found).

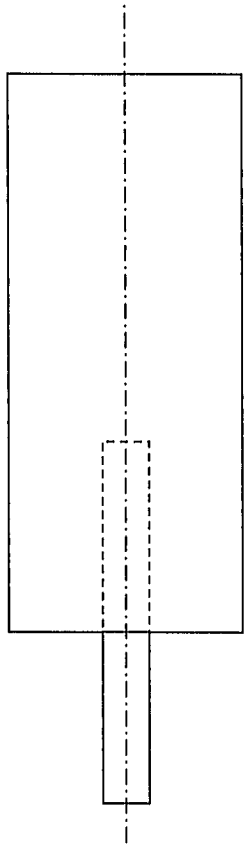

Fig. 4.1a.- Rijke tube

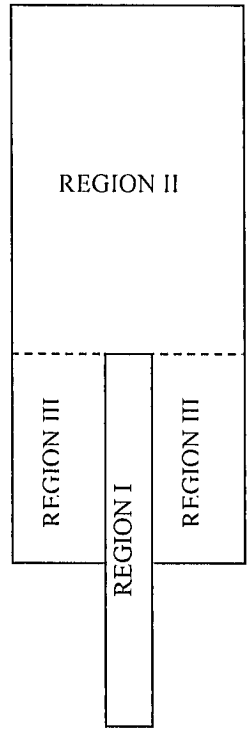

Fig. 4.1b.- Rijke tube regions distribution for study

Region II includes the outer pipe and starts at the point where the inner pipe ends. The pressure at the end of the inner pipe was taken as the source for region II. For this region a 2-D model with axially variable speed of sound was considered. The solution presented is a superposition of a 2-D with constant speed of sound plus a 1-D axially variable speed of sound models. Region III is considered as a 2-D case. The complete solution was found by adding the solutions of regions I, II and III.

4.2. GREEN'S FUNCTION SOLUTION EQUATION FOR THE WAVE EQUATION WITH CONSTANT SPEED OF SOUND

In this part of the work a general Green's function solution equation (GFSE) for the wave equation was developed. Two approaches were given, the first approach was when an oscillatory behavior was assumed for the time; this assumption reduces the wave equation into the Helmholtz equation. The second approach did not consider any assumption for the time. For both approaches one dimensional and two dimensional cases were considered and some elementary problems were solved and compared with other methods for validation purposes of the technique presented here. In addition a pipe with a side branch was analyzed and compared against experimental results. For the side branch problem, a three dimensional model was developed.

During the development of the equations $G(x,t|x',\tau)$ or $p(x,t)$ was written only when necessary to avoid ambiguity or confusion, otherwise just G or p was written for simplicity. For the 1-D Helmholtz approach G means $G(x|x')$. For two-dimensional cases of the wave equation G means $G(x,y,t|x',y',\tau)$ in Cartesian coordinates and $G(r,z,t|r',z',\tau)$ for cylindrical coordinates. For the cylindrical problem it was assumed azimuthally symmetry (i.e. $\frac{\partial}{\partial\theta} = 0$) for all cases in this study except for the side branch pipe case.

4.2.1 One-Dimensional Wave Equation in Rectangular Coordinates

In this section two different GFSE for solving the wave equation are presented. The first approach was done by reducing the wave equation to the Helmholtz equation; the second approach was by solving the wave problem itself.

The one-dimensional homogeneous wave equation in Cartesian coordinates can be found in any acoustics book as:

$$\frac{\partial^2 p}{\partial x^2} - \frac{1}{c^2}\frac{\partial^2 p}{\partial t^2} = 0 \qquad (4.1)$$

Where p is a function of x and t (i.e. p = p(x,t))

4.2.1.1 The Helmholtz Equation

One way of finding a solution for the wave equation is by assuming a periodic solution for the time variable such that:

$$p = \phi . e^{i\omega t} \qquad (4.2)$$

Again, p=p(x,t) and $\Phi=\Phi(x,t)$

By substituting (4.2) in (4.1), the following expression was obtained:

$$\frac{\partial^2 \phi}{\partial x^2} + \frac{\omega^2}{c^2}\phi = 0 \qquad (4.3)$$

Equation (4.3) is the one-dimensional homogeneous Helmholtz equation.

Now consider the non-homogeneous case:

$$\frac{\partial^2 \phi}{\partial x'^2} + \frac{\omega^2}{c^2}\phi = f \qquad (4.4)$$

A change of variable from x to x′ has been done for convenience. In the previous equation the non-homogeneous term f can be also a function of x. Now consider the following non-homogeneous Helmholtz equation:

$$\frac{\partial^2 G}{\partial x'^2} + \frac{\omega^2}{c^2}G = \delta(x'-x) \qquad (4.5)$$

Here G = G(x,x′) is the Green's function and δ(x′-x) is the Dirac-delta function

By multiplying equation (4.4) by G, equation (4.5) by ϕ and subtracting the resulting expressions from each other, the following expression was found:

$$\phi\frac{\partial^2 G}{\partial x'^2} - G\frac{\partial^2 \phi}{\partial x'^2} = \phi\delta(x'-x) - Gf \tag{4.6}$$

Integrating equation (4.6) from 0 to L (where L is the characteristic length of the geometry under study) and after re-arrangement, the following expression was obtained:

$$\int_0^L \phi(x')\delta(x'-x)dx' = \int_0^L \phi\frac{\partial^2 G}{\partial x'^2}dx' - \int_0^L G\frac{\partial^2 \phi}{\partial x'^2}dx' + \int_0^L Gfdx' \tag{4.7}$$

Next, integration of expression (4.7) is performed term by term.

Applying the second of the properties of Dirac-delta function (shown in page 20) to the first term on the left hand side:

$$\int_0^L \phi(x')\delta(x'-x)dx' = \phi(x) \tag{4.7a}$$

By performing integration by parts to the first and second term on the right the following was obtained:

$$\int_0^L \phi\frac{\partial^2 G}{\partial x'^2}dx' = \phi\frac{\partial G}{\partial x'}\Big|_0^L - \int_0^L \frac{\partial G}{\partial x'}\frac{\partial \phi}{\partial x'}dx' \tag{4.7b}$$

$$\int_0^L G\frac{\partial^2 \phi}{\partial x'^2}dx' = G\frac{\partial \phi}{\partial x'}\Big|_0^L - \int_0^L \frac{\partial G}{\partial x'}\frac{\partial \phi}{\partial x'}dx' \tag{4.7c}$$

Substitute (4.7a), (4.7b) and (4.7c) in (4.7) to obtain:

$$\boxed{\phi = \left(\phi\frac{\partial G}{\partial x'}\right)\Big|_0^L - \left(G\frac{\partial \phi}{\partial x'}\right)\Big|_0^L + \int_0^L Gfdx'} \tag{4.8}$$

This last expression is the GFSE for the Helmholtz equation.

Note that the first two terms on the right are evaluated at the ends of the body; therefore, they represent the contribution of the boundary conditions. The last term on the right accounts for the contribution of the source.

Substitute equation (4.8) into equation (4.2) to obtain the solution for the non-homogeneous wave equation provided that the source term F (i.e. the non-homogenous term) can be expressed as $F= f.e^{i(\omega)t}$, which allows the source to be either uniformly distributed or discrete.

4.2.1.2 The Wave Equation

In this section the wave equation is analyzed without being reduced to the Helmholtz equation.

The non-homogeneous case of the wave equation can be expressed as:

$$\frac{\partial^2 p}{\partial x^2} - \frac{1}{c^2}\frac{\partial^2 p}{\partial t^2} = F \tag{4.9}$$

And the auxiliary equation considered for this case was:

$$\frac{\partial^2 G}{\partial x^2} - \frac{1}{c^2}\frac{\partial^2 G}{\partial t^2} = \delta(x-x')\delta(t-\tau) \tag{4.10}$$

In equation (4.9), p is a function of x and t only, which can be renamed to dummy variables x' and τ respectively.

In equation (4.10) G is a function of x, x',t and τ (i.e. $G=G(x,x'|t,\tau)$). Because of the causality principle satisfied by the Green functions, x and x'; t and τ can trade places without affecting the equation.

Therefore, expressions (4.9) and (4.10) can be re-written as:

$$\frac{\partial^2 p}{\partial x'^2} - \frac{1}{c^2}\frac{\partial^2 p}{\partial \tau^2} = F \tag{4.9a}$$

$$\frac{\partial^2 G}{\partial x'^2} - \frac{1}{c^2}\frac{\partial^2 G}{\partial \tau^2} = \delta(x'-x)\delta(\tau - t) \tag{4.10a}$$

Multiply (4.9a) by G, multiply (4.10a) by p and by subtracting the resulting expressions from each other and after re-arrangement the following expression was found:

$$p\delta(x'-x)\delta(\tau - t) = p\frac{\partial^2 G}{\partial x'^2} - G\frac{\partial^2 p}{\partial x'^2} - \frac{1}{c^2}p\frac{\partial^2 G}{\partial \tau^2} + \frac{1}{c^2}G\frac{\partial^2 p}{\partial \tau^2} + G \times F \tag{4.11}$$

Then integrate equation (4.11) in x' and τ from 0 to L and from 0 to (t+ε) respectively, with ε being a very small positive real number. And by performing the integrations in a similar fashion as for the previous case the next expression was obtained:

$$p(x,t) = \int_0^{t+\varepsilon}\left\{\left(p\frac{\partial G}{\partial x'}\right)\Big|_0^L - \left(G\frac{\partial p}{\partial x'}\right)\Big|_0^L\right\}d\tau + \frac{1}{c^2}\int_0^L\left(\left(p\frac{\partial G}{\partial \tau}\right)\Big|_0^{t+\varepsilon} - \left(G\frac{\partial p}{\partial \tau}\right)\Big|_0^{t+\varepsilon}\right)dx' + \int_0^L\int_0^{t+\varepsilon} GF\,d\tau\,dx' \tag{4.12}$$

When integrating in space the starting and ending points are clearly defined; in this particular case the integration was evaluated at distances zero and L therefore the first two terms enclosed in brackets in the right hand side represent the boundary conditions. The situation is different when performing the integration in time. When the integration is evaluated at the "starting point" this is well defined since time zero

represents the initial conditions however, there is not a clearly defined "ending point" since t can be any point in time. Without solving this problem the previous equation can not be used since the two terms in the second bracket on the right hand side could not be evaluated at $\tau = t+\varepsilon$. Therefore the simplification of these terms is critical in the development of the model proposed here.

The two terms of the previous expression under discussion are the following:

$$\left(p\frac{\partial G}{\partial \tau}\right)\Big|_0^{t+\varepsilon} - \left(G\frac{\partial p}{\partial \tau}\right)\Big|_0^{t+\varepsilon} \qquad (*)$$

Following, these terms are analyzed with the help of the Dirac-delta function. From equation (4.10) recall that the Dirac-delta function is given by:

$$\delta(x-x')\delta(t-\tau)$$

Recalling from the general form of the Dirac-delta function $\delta(x-a)$ represents a source of unit strength concentrated around point "a" in space. Similarly $\delta(t-\tau)$ represents the source around point τ in time. When $\tau = 0$ then $(t-\tau) = t$ and the Dirac-delta function becomes $\delta(t)$ which represents the initial impulse and therefore the expression (*) evaluated at time zero becomes the initial conditions.

When $\tau = t+\varepsilon$ then $(t-\tau) = -\varepsilon$. Since ε was defined as a very small real number then a time $-\varepsilon$ represents a time before the impulse. The Green's function is the response of the system to an impulse, but before the impulse there is no response. Therefore expression (*) vanishes when evaluated at $\tau = t+\varepsilon$. Then expression (*) can be re-written as:

$$\left(p\frac{\partial G}{\partial \tau}\right)\Big|_0 - \left(G\frac{\partial p}{\partial \tau}\right)\Big|_0 \qquad (**)$$

Substituting expression (**) and after taking the limit as $\varepsilon \rightarrow 0$, equation (4.12) can be expressed as:

$$p(x,t) = \int_0^t \left\{ \left(p\frac{\partial G}{\partial x'} \right)\Big|_0^{L} - \left(G\frac{\partial p}{\partial x'} \right)\Big|_0^{L} \right\} d\tau + \frac{1}{c^2}\int_0^{L}\left(\left(p\frac{\partial G}{\partial \tau} \right)\Big|_{\tau=0} - \left(G\frac{\partial p}{\partial \tau} \right)\Big|_{\tau=0} \right) dx' + \int_0^{L}\int_0^{t} GF\,d\tau\,dx' \tag{4.13}$$

Equation (4.13) is the GFSE for the 1-D wave equation. The first integral on the right hand side represents the contribution of the boundary conditions; the second term represents the contribution of the initial conditions and the last one is the contribution of the source, therefore this is a general solution for the 1-D wave equation.

Again, note that no restrictions were applied to the source during the derivation of the GFSE, therefore, the source can be a function of x, t, or both and can be either uniformly distributed or discrete. The GFSE is even valid for the case of zero source (i.e. homogeneous problem).

4.2.2 Two-Dimensional Wave Equation

4.2.2.1. Cartesian Coordinates

The two-dimensional wave equation is given by:

$$\frac{\partial^2 p}{\partial x^2} + \frac{\partial^2 p}{\partial y^2} - \frac{1}{c^2}\frac{\partial^2 p}{\partial t^2} = F \tag{4.14a}$$

And the auxiliary equation is given by:

$$\frac{\partial^2 G}{\partial x^2} + \frac{\partial^2 G}{\partial y^2} - \frac{1}{c^2}\frac{\partial^2 G}{\partial t^2} = \delta(x - x'/\, y - y')\delta(t - \tau) \tag{4.14b}$$

By following the same procedure previously used for the one-dimensional case, the next expressions were found:

For the Helmholtz approach:

$$\phi(x,y)=\int_0^{H}\left\{\left(\phi\frac{\partial G}{\partial x'}\right)\Big|_0^{L}-\left(G\frac{\partial \phi}{\partial x'}\right)\Big|_0^{L}\right\}dy'+\int_0^{L}\left\{\left(\phi\frac{\partial G}{\partial y'}\right)\Big|_0^{L}-\left(G\frac{\partial \phi}{\partial y'}\right)\Big|_0^{L}\right\}dx'+\int_0^{H}\int_0^{L}Gf dx'dy' \quad (4.15)$$

And for the wave equation:

$$p(x,y,t)=\int_0^{t}\int_0^{H}\left\{\left(p\frac{\partial G}{\partial x'}\right)\Big|_0^{L}-\left(G\frac{\partial p}{\partial x'}\right)\Big|_0^{L}\right\}dy'd\tau+\int_0^{t}\int_0^{L}\left\{\left(p\frac{\partial G}{\partial y'}\right)\Big|_0^{H}-\left(G\frac{\partial p}{\partial y'}\right)\Big|_0^{H}\right\}dx'd\tau+$$

$$\frac{1}{c^2}\int_0^{H}\int_0^{L}\left(\left(p\frac{\partial G}{\partial \tau}\right)\Big|_{\tau=0}-\left(G\frac{\partial p}{\partial \tau}\right)\Big|_{\tau=0}\right)dx'dy'+\int_0^{H}\int_0^{L}\int_0^{t}GFd\tau dx'dy' \quad (4.16)$$

Integration was considered from 0 to L in the x direction and from 0 to H in the y direction. L and H are the characteristic lengths of the geometry. Here, the two terms in the first double integral on the right hand side represent the contribution of the boundary conditions on the x axis; the two terms on the second double integral represent the contribution of the boundary conditions on the y axis; the two terms on the third double integral represent the contribution of the initial conditions, and the triple integral represents the contribution of the source.

4.2.2.2. Cylindrical Coordinates

The two-dimensional wave equation in cylindrical coordinates for the case with radial and axial dependence is given by:

$$\frac{1}{r}\frac{\partial}{\partial r}\left(r\frac{\partial p}{\partial r}\right)+\frac{\partial^2 p}{\partial z^2}-\frac{1}{c^2}\frac{\partial^2 p}{\partial t^2}=F \tag{4.17}$$

The auxiliary equation used for this case was:

$$\frac{1}{r}\frac{\partial}{\partial r}\left(r\frac{\partial G}{\partial r}\right)+\frac{\partial^2 G}{\partial z^2}-\frac{1}{c^2}\frac{\partial^2 G}{\partial t^2}=\delta(r-r')\delta(z-z')\delta(t-\tau) \tag{4.18}$$

The GFSE was obtained to be:

$$p(r,z,t)=\int_0^t\int_0^L r_0\left\{\left(p\frac{\partial G}{\partial r'}\right)\Big|_{r'=r_0}-\left(G\frac{\partial p}{\partial r'}\right)\Big|_{r'=r_0}\right\}dz'd\tau+\int_0^t\int_0^{r_0}\left\{\left(p\frac{\partial G}{\partial z'}\right)\Big|_0^L-\left(G\frac{\partial p}{\partial z'}\right)\Big|_0^L\right\}r'dr'd\tau+$$
$$\frac{1}{c^2}\int_0^L\int_0^{r_0}\left(\left(p\frac{\partial G}{\partial \tau}\right)\Big|_{\tau=0}-\left(G\frac{\partial p}{\partial \tau}\right)\Big|_{\tau=0}\right)r'dr'dz'+\int_0^t\int_0^L\int_0^{r_0}GFr'dr'dz'd\tau \tag{4.19}$$

Here r_0 is the characteristic radius of the cylindrical geometry under study.

Equation (4.19) was found under the same procedure as before. Just notice that the integration was performed including the Sturm-Liouville weight function "r" [53] (i.e. $\int f(r,z)rdrdz$).

NOTE: A detailed development of the GFSE for cylindrical coordinates is given for the 3-D case when the side branch pipe problem is analyzed.

By assuming a periodic behavior in time, the cylindrical Helmholtz version was also obtained as follows:

$$\phi(r,z) = \int_0^L r_0 \left\{ \left(p \frac{\partial \phi}{\partial r'} \right)\Big|_{r'=r_0} - \left(G \frac{\partial \phi}{\partial r'} \right)\Big|_{r'=r_0} \right\} dz' + \int_0^{r_0} \left(\left(\phi \frac{\partial G}{\partial z} \right)\Big|_0^L - \left(G \frac{\partial \phi}{\partial \tau} \right)\Big|_0^L \right) r' dr' + \int_0^L \int_0^{r_0} G f r' dr' dz' \tag{4.20}$$

4.3. GREEN'S FUNCTION SOLUTION EQUATION FOR THE WAVE EQUATION WITH AXIALLY VARIABLE SPEED OF SOUND

Up to this point it was assumed that the speed of sound c was constant along the body under study. All the previous equations were derived with this consideration. Although this assumption is useful and give excellent results for some cases, it may fail when the calculation is perform for an environment where the temperature profile varies significantly. This is the case when combustion takes place inside the geometry under investigation.

It is well known that the speed of sound of gases is a function of its temperature. For ideal gases the dependency of the speed of sound with respect to its temperature is given by the following equation:

$$c = \sqrt{\gamma . R . T} \ \text{(m/s)} \tag{4.21}$$

Where γ is the ratio of specific heats, R is the gas constant and T is the temperature in Kelvin.

Now a temperature profile varying along the x-axis or axially for the Cartesian and cylindrical coordinates respectively is considered. For varying speeds of sound the wave equations were found to be:

For 2-D Cartesian coordinates:

$$\frac{\partial}{\partial x}\left(c^2\frac{\partial p}{\partial x}\right)+c^2\frac{\partial^2 p}{\partial y^2}-\frac{\partial^2 p}{\partial t^2}=0 \tag{4.22}$$

For 2-D Cylindrical coordinates:

$$c^2\frac{1}{r}\frac{\partial}{\partial r}\left(r\frac{\partial p}{\partial r}\right)+\frac{\partial}{\partial x}\left(c^2\frac{\partial p}{\partial x}\right)-\frac{\partial^2 p}{\partial t^2}=0 \tag{4.23}$$

In this section c = c(x) since c is a function of temperature and it is assumed that the temperature varies along x.

By following the same procedure as the previous cases the GFSE were found as shown:

$$p(x,t)=\int_0^t\left\{\left(c^2p\frac{\partial G}{\partial x'}\right)\Big|_0^L-\left(c^2G\frac{\partial p}{\partial x'}\right)\Big|_0^L\right\}d\tau+\int_0^L\left(\left(p\frac{\partial G}{\partial \tau}\right)\Big|_{\tau=0}-\left(G\frac{\partial p}{\partial \tau}\right)\Big|_{\tau=0}\right)dx'+\int_0^L\int_0^t GFd\tau dx' \tag{4.24}$$

Equation (4.24) is the GFSE for 1-D in cylindrical coordinates with speed of sound varying axially. This equation is also valid for 1-D Cartesian coordinates.

$$p(x,y,t)=\int_0^t\int_0^H\left\{\left(c^2p\frac{\partial G}{\partial x'}\right)\Big|_0^L-\left(c^2G\frac{\partial p}{\partial x'}\right)\Big|_0^L\right\}dy'd\tau+\int_0^t\int_0^L c^2\left\{\left(p\frac{\partial G}{\partial y'}\right)\Big|_0^H-\left(G\frac{\partial p}{\partial y'}\right)\Big|_0^H\right\}dx'd\tau+$$
$$\int_0^H\int_0^L\left(\left(p\frac{\partial G}{\partial \tau}\right)\Big|_{\tau=0}-\left(G\frac{\partial p}{\partial \tau}\right)\Big|_{\tau=0}\right)dx'dy'+\int_0^H\int_0^L\int_0^t GFd\tau dx'dy' \tag{4.25}$$

Equation (4.25) is the 2-D GFSE for the wave equation in Cartesian coordinates with the speed of sound varying along the x axis.

$$p(r,x,t)=\int_0^t\int_0^L c^2R\left\{\left(p\frac{\partial G}{\partial r'}\right)\Big|_{r'=R}-\left(G\frac{\partial p}{\partial r'}\right)\Big|_{r'=R}\right\}dx'd\tau+\int_0^t\int_0^R\left\{\left(c^2p\frac{\partial G}{\partial x'}\right)\Big|_0^L-\left(c^2G\frac{\partial p}{\partial x'}\right)\Big|_0^L\right\}r'dr'd\tau+$$

$$\int_0^L\int_0^R\left(\left(p\frac{\partial G}{\partial \tau}\right)\Big|_{\tau=0}-\left(G\frac{\partial p}{\partial \tau}\right)\Big|_{\tau=0}\right)r'dr'dx'+\int_0^t\int_0^L\int_0^R GFr'dr'dx'd\tau \qquad (4.26)$$

Equation (4.26) is the 2-D GFSE for the wave equation in cylindrical coordinates with the speed of sound varying along the axis of the cylinder.

Notice the similitude of these equations with their pairs for constant speed of sound. In these cases the speed of sound was integrated together with p, G or its derivatives. In other terms the speed of sound is evaluated at the boundaries.

4.4. FINDING THE GREEN'S FUNCTIONS

Equations (4.8), (4.13), (4.15), (4.16), (4.19) and (4.20) are the GFSE's for the wave equation for the different cases considered above. All these expressions are the general solution to the wave equation for one and 2-D in Cartesian and cylindrical coordinates. These solutions are expressed as function of the boundary values, the initial conditions, the source and the Green's function. Boundary and initial values for a given problem have to be known, also the source is known if the problem is non-homogeneous, therefore the next unknown to be determined is the Green's function itself which depends on the problem at hand.

But how can the GF be found? The next pages are devoted to illustrate the process of finding the GF. Only two cases are presented here, one for 1-D in Cartesian coordinates with constant speed of sound plus a 1-D case with variable speed of sound.

Several 1-D and 2-D cases in Cartesian and cylindrical coordinates can be found in Appendix B.

4.4.1 GF For The 1-D Wave Equation With Dirichlet Boundary Conditions and Constant Speed Of Sound In Cartesian Coordinates:

Consider the homogeneous one-dimensional problem for a body of length L, with no sources and the following Dirichlet (or first kind) boudary conditions:

Boundary conditions: $p(0,t)=0$ (4.27a)

$p(L,t)=0$ (4.27b)

Initial conditions: $p(x,0)=h(x)$ (4.27c)

$p_t(x,0)=g(x)$ (4.27d)

The problem can be solved by the classical separation of variables method. A fully explanation of the separation of variables method can be easily found in any advanced mathematics, Heat Conduction or other applied Mathematics books such as [18], [22], [52], and [53]. Because of its importance, during the process of finding the GF the separation of variables technique is revisited in this part without further details.

Recall the 1-D homogeneous wave equation:

$$\frac{\partial^2 p}{\partial x^2} - \frac{1}{c^2}\frac{\partial^2 p}{\partial t^2} = 0$$

Assuming that the solution is the product of two new functions of a single variable as shown (for the 2-D case the solution is assumed to be the product of three functions, one for x and one for y in space plus one function for time):

$$p(x,t) = X(x).\Gamma(t) \quad (4.28)$$

By substituting these two functions into the wave equation, then dividing by X.Γ and after re-arrangement, the following expression was obtained:

$$\frac{X''}{X} = \frac{1}{c^2}\frac{\Gamma''}{\Gamma} \tag{4.29}$$

Since the first term on the right is only a function of x and the second term is only a function of t the only way of this to be true is if and only if they both are equal to a constant. For convenience the constant chosen is $-k^2$ where k is a real number.

Therefore:

$$\frac{X''}{X} = -k^2 \tag{4.30a}$$

And

$$\frac{1}{c^2}\frac{\Gamma''}{\Gamma} = -k^2 \tag{4.30b}$$

Typical solutions for these kinds of expressions are:

$$X(x) = a_1.\sin(kx) + a_2.\cos(kx) \tag{4.31a}$$

$$\Gamma(t) = b_1.\sin(\omega t) + b_2\cos(\omega t) \tag{4.31b}$$

Where a_1, a_2, b_1, b_2 are constants to be determined after applying the boundary and initial conditions and ω=kc is the angular frequency.

By applying boundary condition (4.27a) it was found that $a_2 = 0$ and by applying the boundary condition (4.21b) it was determined that $k = \frac{n\pi}{L}$ with n= 1,2,3...

The complete solution to the problem is the summation of all values of n. By substitution of these constants into expression (4.31a) and with expression (4.31b) in equation (4.28) the following was obtained:

$$p(x,t) = \sum_{n=1}^{\infty} \sin\left(\frac{n\pi}{L}x\right)\left[b_1 \sin\left(\frac{n\pi}{L}c.t\right) + b_2 \cos\left(\frac{n\pi}{L}c.t\right)\right] \tag{4.32}$$

In this last expression the constant a_1 has been absorbed by b_1 and b_2.

Applying the initial conditions (4.27c) and (4.27d) to equation (4.32) the following expressions were obtained:

$$h(x) = \sum_{n=1}^{\infty} b_2 \sin\left(\frac{n\pi}{L}x\right) \tag{4.33a}$$

$$g(x) = \sum_{n=1}^{\infty} b_1\left(\frac{n\pi}{L}c\right).\sin\left(\frac{n\pi}{L}x\right) \tag{4.33b}$$

By applying orthogonality of functions to equations (4.33a) and (4.33b) the constants b_1 and b_2 were found respectively as:

$$b_1 = \frac{2}{n\pi.c}\int_0^L g(x')\sin(x')dx' \tag{4.34a}$$

$$b_2 = \frac{2}{L}\int_0^L h(x')\sin(x')dx' \tag{4.34b}$$

After substitution of expressions (4.34a) and (4.34b) into equation (4.32) and further re-arrangement the solution to the problem was obtained as:

$$p(x,t) = \int_0^L \frac{2}{\omega L}\sum_{n=1}^{\infty}\sin(kx)\sin(\omega t)\sin(kx')g(x')dx' + \int_0^L \frac{2}{L}\sum_{n=1}^{\infty}\sin(kx)\cos(\omega t)\sin(kx')h(x')dx' \tag{4.35}$$

Where: $k = \frac{n\pi}{L}$

And

$$\omega = kc = \frac{n\pi}{L}c$$

Equation (4.35) is the solution for the 1-D wave equation with no sources with Dirichlet boundary conditions and initial conditions (4.27c) and (4.27d).

Next, the same problem was solved by applying the GFSE. Recall the GFSE for the 1-D case, equation (4.12):

$$p(x,t) = \int_0^t \left\{ \left(p\frac{\partial G}{\partial x'} \right)\Big|_0^L - \left(G\frac{\partial p}{\partial x'} \right)\Big|_0^L \right\} d\tau + \frac{1}{c^2}\int_0^L \left(\left(p\frac{\partial G}{\partial \tau} \right)\Big|_{\tau=0} - \left(G\frac{\partial p}{\partial \tau} \right)\Big|_{\tau=0} \right) dx' + \int_0^L \int_0^t GF\,d\tau\,dx'$$

The usual practice is, conveniently, to choose the boundary conditions for the auxiliary problem to be homogeneous and of the same kind of the boundary value problem to be solved. In this case $G(x,t|0,\tau) = G(x,t|L,\tau) = 0$

Recall that p=p(x,t). Since the two terms in the first integral are evaluated at x=0 and x=L then p(x,t) becomes p(0,t) and p(L,t) which are equal to zero since they are the boundary conditions. Therefore the two terms on the first integral vanishes. Similarly the last term on the double integral vanishes since F = 0 (i.e. no source). After applying all these simplifications equation (4.12) becomes:

$$p(x,t) = \frac{1}{c^2}\int_0^L \left(\left(p\frac{\partial G}{\partial \tau} \right)\Big|_{\tau=0} - \left(G\frac{\partial p}{\partial \tau} \right)\Big|_{\tau=0} \right) dx' \qquad (4.36)$$

Furthermore, the two terms inside the integral are evaluated at time zero therefore they represent the initial conditions. Then $p(x,0) = h$ and $p_t(x,0) = g$ therefore equation (4.36) becomes:

$$p(x,t) = \frac{1}{c^2}\int_0^L h(x')\left(\frac{\partial G}{\partial \tau} \right)\Big|_{\tau=0} dx' - \frac{1}{c^2}\int_0^L g(x')(G)\Big|_{\tau=0} dx' \qquad (4.37)$$

Equations (4.35) and (4.37) are the solutions to the same problem. By comparing these expressions it can be concluded that:

$$\boxed{G = \sum_{n=1}^{\infty} \frac{-2c}{n\pi} \sin(kx') \sin(kx) \sin(\omega[t-\tau])} \tag{4.38}$$

Were:

$$k = \frac{n\pi}{L} \qquad \text{and} \qquad \omega = kc$$

Equation (4.38) is the GF for the 1-D wave equation with Dirichlet boundary conditions. This GF is valid whether the problem is homogeneous or not.

Notice that the GF was found from the solution of the homogeneous case with homogeneous boundary conditions. These kinds of problems are relatively simple to solve. Then the GF can be applied to the GFSE to solve more complex problems.

Using a similar procedure as the case discussed above, the problem of the wave equation with various homogeneous boundary conditions can be solved and provide the GF. Several GF's for one and two dimensional cases in Cartesian and cylindrical coordinates can be found in Appendix B.

4.4.2. GF For The 1-D Wave Equation With Dirichlet Boundary Conditions And Variable Speed Of Sound In Cartesian Coordinates:

From equation (4.22) the 1-D wave equation in Cartesian coordinates for varying speeds of sound was obtained when no variation in the "y" direction was considered. This equation can be expressed as:

$$\frac{\partial}{\partial x}\left(c^2\frac{\partial p}{\partial x}\right)-\frac{\partial^2 p}{\partial t^2}=0 \tag{4.39}$$

Notice that the same expression can be obtained from equation (4.23) when there is no change in the radial direction therefore equation (4.39) is valid for axially varying speed of sound in cylindrical coordinates.

Since the speed of sound c is a function of x, equation (4.39) can be expanded to obtain the following expression:

$$c^2\frac{\partial^2 p}{\partial x^2}+2c\frac{\partial c}{\partial x}\frac{\partial p}{\partial x}-\frac{\partial^2 p}{\partial t^2}=0 \tag{4.40}$$

By assuming a solution of the form:

$$p(x,t)=X(x).\Gamma(t) \tag{4.41}$$

Applying the separation of variables technique the solution for the time dependant part of the problem and a differential equation for the space dependant part were obtained as:

$$\Gamma(t)=a_1.\sin(\omega t)+b_1.\cos(\omega t) \tag{4.42}$$

$$c^2\frac{d^2}{dx^2}[X(x)]+2c\frac{dc}{dx}.\frac{d}{dx}[X(x)]+\omega^2 X(x)=0 \tag{4.43}$$

Since neither initial conditions nor boundary conditions have been specified, equations (4.42) and (4.43) are valid for any kind of boundary and initial conditions. Furthermore, these equations are also valid for any temperature profile, in other words valid for any speed of sound profile as long as this varies only with distance.

4.4.2.1. Parabolic Temperature Profile

Consider the case where the temperature profile is given by:

$$T(x) = a.(b.x + 1)^2 \tag{4.44}$$

Where "a" and "b" are constants.

By substitution of equation (4.44) into equation (4.21) the speed of sound c can be expressed as:

$$c = \sqrt{\gamma.R.a.(b.x+1)^2} = \sqrt{\xi}(b.x+1) \tag{4.45}$$

Where $\xi = \gamma.R.a$ (4.46)

After substitution of equation (4.45) into (4.43) the following expression was obtained:

$$\xi.(b.x+1)^2 \frac{d^2}{dx^2}[X(x)] + 2.b.\xi.(b.x+1)\frac{d}{dx}[X(x)] + \omega^2 X(x) = 0 \tag{4.47}$$

Defining a new variable:

$$z = \frac{1}{b}\ln|b.x+1| \tag{4.48}$$

Substitute the new variable z from equation (4.48) into equation (4.47), with the use of the chain rule and some simplifications, the following was obtained:

$$\frac{d^2}{dz^2}[Z(z)] + b\frac{d}{dz}[Z(z)] + \frac{\omega^2}{\xi}Z(z) = 0 \tag{4.49}$$

Equation (4.49) is an ODE with constant coefficients and its characteristic equation is given by:

$$m = \frac{1}{2}\left[-b \pm \sqrt{b^2 - 4\frac{\omega^2}{\xi}}\right] \tag{4.50}$$

Let D be the determinant, then:

$$D = b^2 - 4\frac{\omega^2}{\xi} \tag{4.51}$$

$$\text{Then} \quad m = \frac{1}{2}\left[-b \pm \sqrt{D}\right] \tag{4.52}$$

Three possibilities for the solution in the space domain can be obtained from the characteristic equation depending on the values of the parameters in the determinant D. These solutions are as follow:

If D = 0

$$Z(z) = A.e^{\frac{-b}{2}z} + B.z.e^{\frac{-b}{2}z} \tag{4.53a}$$

If D>0

$$Z(z) = e^{\frac{-b}{2}z}\left[A.\sinh\left(\frac{\sqrt{D}}{2}z\right) + B.\cosh\left(\frac{\sqrt{D}}{2}z\right)\right] \tag{4.53b}$$

If D<0

$$Z(z) = e^{\frac{-b}{2}z}\left[A.\sin\left(\frac{\sqrt{-D}}{2}z\right) + B.\cos\left(\frac{\sqrt{-D}}{2}z\right)\right] \tag{4.53c}$$

Or by substituting back x and D expressions (4.53a), (4.53b) and (4.53c) can be re-written as:

If D=0

$$X(x) = A\frac{1}{\sqrt{b.x+1}} + B\frac{\ln|b.x+1|}{b.\sqrt{bx+1}} \tag{4.54a}$$

If D>0

$$X(x)=\frac{1}{\sqrt{b.x+1}}\left[A.\sinh\left(\frac{1}{2b}\sqrt{\left\{b^2-4\frac{\omega^2}{\xi}\right\}}\ln|b.x+1|\right)+B.\cosh\left(\frac{1}{2b}\sqrt{\left\{b^2-4\frac{\omega^2}{\xi}\right\}}\ln|b.x+1|\right)\right] \quad (4.54b)$$

If D<0

$$X(x)=\frac{1}{\sqrt{b.x+1}}\left[A.\sin\left(\frac{1}{2b}\sqrt{\left\{4\frac{\omega^2}{\xi}-b^2\right\}}\ln|b.x+1|\right)+B.\cos\left(\frac{1}{2b}\sqrt{\left\{4\frac{\omega^2}{\xi}-b^2\right\}}\ln|b.x+1|\right)\right] \quad (4.54c)$$

The boundary conditions of interest for this study are of first kind, second kind or a combination of both. The most important cases are those where both boundary conditions are of the first kind and the case where one boundary condition is of first kind and the other of second kind.

Consider the boundary conditions given by equations (4.27a) and (4.27b); and the initial conditions given by equations (4.27c) and (4.27d).

The boundary conditions imply:

$$X(0) = 0 \qquad \text{and} \qquad X(L) = 0 \quad (4.55)$$

An analysis of each possible value of D is shown next:

CASE I: D = 0

Equation (4.54a) is the mathematical solution for case D=0 but the boundary conditions given by (4.55) are satisfied only if the constants A and B are equal to zero which leads to a trivial solution.

CASE II: D>0

The mathematical solution for this case is given by equation (4.54b). Again, consider the same boundary conditions given by (4.55). Similarly to the previous case the

boundary conditions are satisfied only if the constants A and B are equal to zero leading to a trivial solution.

CASE III: D<0

When D<0 the solution for the space domain is given by (4.54c). Consider the boundary conditions given by (4.55). The boundary condition Z(0)=0 (or its equivalent X(0) = 0) is satisfied only if B=0 then the solution is reduced to:

$$Z(z) = A.e^{\frac{-b}{2}z}.\sin\left(\frac{\sqrt{-D}}{2}z\right) \tag{4.56}$$

Or

$$X(x) = A.\frac{1}{\sqrt{b.x+1}}.\sin\left(\frac{1}{2b}\sqrt{\left\{4\frac{\omega^2}{\xi}-b^2\right\}}\ln|b.L+1|\right) = 0 \tag{4.57}$$

By applying the boundary condition at x=L equation (4.57) is satisfied only if:

$$\frac{1}{2b}\sqrt{\left\{4\frac{\omega^2}{\xi}-b^2\right\}}\ln|b.L+1| = n\pi \qquad \text{n=1,2,3...} \tag{4.58}$$

By solving for ω the eigenfrecuencies were obtained as:

$$\omega = \frac{1}{2}\sqrt{\gamma.R.a\left(\left[\frac{2n\pi b}{\ln|bL+1|}\right]^2 + b^2\right)} \tag{4.59}$$

The complete solution was obtained by substitution of equations (4.42) and (4.57) into equation (4.41) and considering all values of n accordingly with the separation of variables technique. The expression obtained was the following:

$$p(x,t) = \sum_{n=1}^{\infty}\frac{1}{\sqrt{b.x+1}}.\sin\left(\frac{1}{2b}\sqrt{\left\{4\frac{\omega^2}{\xi}-b^2\right\}}\ln|b.x+1|\right)\left(a_1.\sin(\omega.t)+b_1.\cos(\omega.t)\right) \tag{4.60}$$

In equation (4.60) the constant A from expression (4.57) have been absorbed by the constants a_1 and b_1.

NOTE: Other combinations of boundary conditions were also applied to equations (4.53a) and (4.53b) showing that they are not possible solutions. Therefore the only allowed solution is given by equation (4.53c). Therefore the complete solution for the acoustic pressure for any combination of first and second kind boundary conditions is given by:

$$P(x,t)=\frac{1}{\sqrt{b.x+1}}\left[A.\sin\left(\frac{1}{2b}\sqrt{-D}\,\ln|b.x+1|\right)+B.\cos\left(\frac{1}{2b}\sqrt{-D}\,\ln|b.x+1|\right)\right]\{a_1\sin(\omega.t)+b_1\cos(\omega.t)\} \tag{4.61}$$

The values of A_n and B_n will depend on the given boundary and initial conditions.

By applying the initial condition (4.27c) and (4.27d) the following expressions were obtained:

$$h(x)=\sum_{n=1}^{\infty}b_1.\frac{1}{\sqrt{b.x+1}}.\sin\left(\frac{1}{2b}\sqrt{\left\{4\frac{\omega^2}{\xi}-b^2\right\}}\ln|b.x+1|\right) \tag{4.62a}$$

$$g(x)=\sum_{n=1}^{\infty}a_1.\frac{\omega}{\sqrt{b.x+1}}.\sin\left(\frac{1}{2b}\sqrt{\left\{4\frac{\omega^2}{\xi}-b^2\right\}}\ln|b.x+1|\right) \tag{4.62b}$$

At this point is more convenient to express these last two equations in terms of the new variable z as:

$$h(z)=\sum_{n=1}^{\infty}b_1.e^{-\frac{b}{2}z}.\sin\left(\frac{1}{2}\sqrt{\left\{4\frac{\omega^2}{\xi}-b^2\right\}}z\right) \tag{4.63a}$$

$$g(z)=\sum_{n=1}^{\infty} a_1.\omega.e^{-\frac{b}{2}z}.\sin\left(\frac{1}{2}\sqrt{\left\{4\frac{\omega^2}{\xi}-b^2\right\}}z\right) \tag{63.b}$$

Constants a_1 and b_1 were found from these last two equations with the use of orthogonality of functions obtaining the following expressions:

$$a_1=\frac{2.\omega}{z_L}\int_0^{z_L} g(z).e^{\frac{b}{2}z}.\sin\left(\frac{1}{2}\sqrt{\left\{4\frac{\omega^2}{\xi}-b^2\right\}}.z\right)dz \tag{4.64a}$$

$$b_1=\frac{2}{z_L}\int_0^{z_L} h(z).e^{\frac{b}{2}z}.\sin\left(\frac{1}{2}\sqrt{\left\{4\frac{\omega^2}{\xi}-b^2\right\}}.z\right)dz \tag{4.64b}$$

Where $z_L=\frac{1}{b}\ln|b.L+1|$ was obtained from equation (4.48) when x=L. By returning to the original variable x, equations (4.64a) and (4.64b) can be expressed as:

$$a_1=\frac{2b.\omega}{\ln|bL+1|}\int_0^{L} g(x).\sqrt{|b.x+1|}.\sin\left(\frac{1}{2.b}\sqrt{\left\{4\frac{\omega^2}{\xi}-b^2\right\}}.\ln|bx+1|\right)dx \tag{4.65a}$$

$$b_1=\frac{2b}{\ln|bL+1|}\int_0^{L} h(x).\sqrt{|b.x+1|}.\sin\left(\frac{1}{2.b}\sqrt{\left\{4\frac{\omega^2}{\xi}-b^2\right\}}.\ln|bx+1|\right)dx \tag{4.65b}$$

$$p(x,t)=\sum_{n=1}^{\infty}\begin{pmatrix}\frac{2b.\omega}{\ln|bL+1|}\int_0^{L} g(x').\sin\left(\frac{1}{2.b}\sqrt{\left\{4\frac{\omega^2}{\xi}-b^2\right\}}.\ln|bx'+1|\right).\frac{\sqrt{|b.x'+1|}}{\sqrt{|b.x+1|}}.\sin\left(\frac{1}{2b}\sqrt{\left\{4\frac{\omega^2}{\xi}-b^2\right\}}\ln|b.x+1|\right)\sin(\omega.t)dx'+\ldots\\ \frac{2b}{\ln|bL+1|}\int_0^{L} h(x').\sin\left(\frac{1}{2.b}\sqrt{\left\{4\frac{\omega^2}{\xi}-b^2\right\}}.\ln|bx'+1|\right).\frac{\sqrt{|b.x'+1|}}{\sqrt{|b.x+1|}}.\sin\left(\frac{1}{2b}\sqrt{\left\{4\frac{\omega^2}{\xi}-b^2\right\}}\ln|b.x+1|\right)\cos(\omega.t)dx'\end{pmatrix} \tag{4.66}$$

Solving the same problem with the use of the GFSE equation (4.24) considering the boundary conditions given by (4.27a) and (4.27b) and no source the following expression was obtained:

$$p(x,t)=\int_0^{L}\left(\left(p\frac{\partial G}{\partial \tau}\right)\Big|_{\tau=0}-\left(G\frac{\partial p}{\partial \tau}\right)\Big|_{\tau=0}\right)dx' \tag{4.67}$$

By comparing equations (4.66) and (4.67) it can be extracted the Green's function for the case under discussion:

$$G=\sum_{n=1}^{\infty}\left(\frac{2b.\omega}{\ln|bL+1|}..\sin\left(\frac{1}{2.b}\sqrt{\left\{4\frac{\omega^2}{\xi}-b^2\right\}}.\ln|bx'+1|\right).\frac{\sqrt{|b.x'+1|}}{\sqrt{|b.x+1|}}.\sin\left(\frac{1}{2b}\sqrt{\left\{4\frac{\omega^2}{\xi}-b^2\right\}}\ln|b.x+1|\right)\sin(\omega.[t-\tau])\right) \tag{4.68}$$

Where:

$$\omega=\frac{1}{2}\sqrt{\gamma.R.a\left(\left[\frac{2n\pi b}{\ln|bL+1|}\right]^2+b^2\right)} \tag{4.68a}$$

Equation (4.68) is the GF for the 1-D wave equation with variable speed of sound with parabolic profile and Dirichlet boundary conditions.

CHAPTER V

RESULTS AND DISCUSSION

In order to validate the technique proposed in the present work some simple cases were solved in this chapter. The results obtained using the Green's functions technique were then compared with the results found in the literature. The case of a pipe with a side branch pipe was also solved and compared with experimental data.

5.1. ONE-DIMENSIONAL TRIANGULAR INITIAL DISTRIBUTION

Consider the initial distribution given by equation (5.1) and shown in figure 5.1 below:

$$p(x,0) = f(x) = \begin{cases} \frac{2\alpha}{L}x & 0 \le x < L/2 \\ \frac{2\alpha}{L}(L-x) & L/2 \le x \le L \end{cases} \tag{5.1}$$

$$p_t(x,0) = g(x) = 0 \tag{5.2}$$

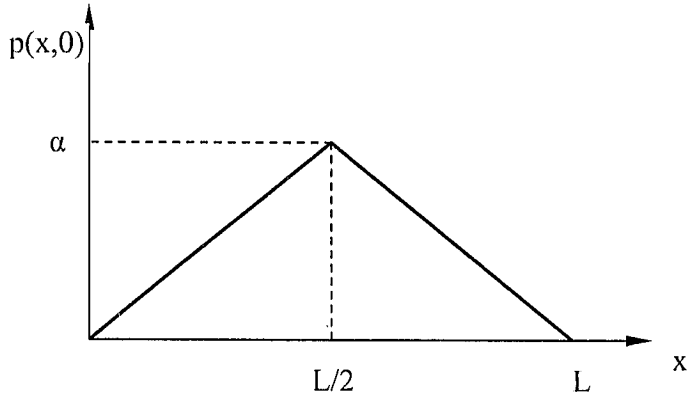

Fig.5.1. Initial triangular distribution equation (4.69)

The boundary conditions considered for this case were of the first kind given by: $p(0,t) = p(L,t) = 0$.

Since this is a 1-D problem in Cartesian coordinates the corresponding GFSE is given by equation (4.13) recalled below:

$$p(x,t) = \int_0^t \left\{ \left(p\frac{\partial G}{\partial x'} \right)\Big|_0^L - \left(G\frac{\partial p}{\partial x'} \right)\Big|_0^L \right\} d\tau + \frac{1}{c^2}\int_0^L \left(\left(p\frac{\partial G}{\partial \tau} \right)\Big|_{\tau=0} - \left(G\frac{\partial p}{\partial \tau} \right)\Big|_{\tau=0} \right) dx' + \int_0^L \int_0^t GF\, d\tau\, dx'$$

First and second terms on the right hand side are equal to zero because those terms are evaluated at x=0 and x=L corresponding to the boundary conditions. The fourth term is also equal to zero because of initial condition equation (5.2). Fifth term is also eliminated since there are not sources. Therefore for this case the GFSE equation was reduced to the following:

$$p(x,t) = \frac{1}{c^2}\int_0^L \left(p\frac{\partial G}{\partial \tau} \right)\Big|_{\tau=0} dx' \tag{5.3}$$

Equation (4.38) is the GF for the 1-D wave equation with Dirichlet boundary conditions. After substitution of equations (4.38) and (5.1) into expression (5.3) the following was obtained:

$$p(x,t) = \int_0^{L/2} \left(\frac{\partial}{\partial \tau} \sum_{n=1}^{\infty} \frac{4\alpha.}{n\pi cL} x'.\sin(kx')\sin(kx)\sin(\omega[t-\tau]) \right) dx' + \ldots$$

$$\int_0^{L/2} \left(\frac{\partial}{\partial \tau} \sum_{n=1}^{\infty} \frac{4\alpha.}{n\pi cL} (L-x').\sin(kx')\sin(kx)\sin(\omega[t-\tau]) \right) dx' \tag{5.4}$$

After performing the integrations and some simplifications of the expressions, the result was obtained as:

$$p(x,t) = \sum_{n=1}^{\infty} \frac{8\alpha}{(n\pi)^2} \sin\left(\frac{n\pi}{2}\right) \sin\left(\frac{n\pi}{L}x\right) \cos\left(\frac{n\pi}{L}ct\right) \qquad (5.5)$$

The solution to this problem can be found also in Krayzig [52] and the result is presented as:

$$p(x,t) = \sum_{n=1}^{\infty} \frac{8\alpha}{\pi^2}\left(\frac{1}{1^2}\sin\left(\frac{\pi}{L}x\right)\cos\left(\frac{\pi}{L}ct\right) - \frac{1}{3^2}\sin\left(\frac{3\pi}{L}x\right)\cos\left(\frac{3\pi}{L}ct\right) + -\ldots\right) \qquad (5.6)$$

Equation (5.6) is an equivalent expression to equation (5.5) which was obtained using the Green's functions technique. Figure (5.2) below shows plotting of results for equations (5.5) and (5.6) for several values of time. Both results are exactly the same and lines superimpose to each other.

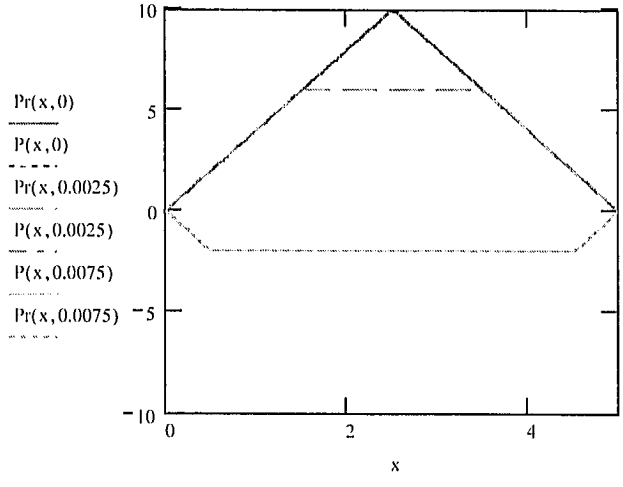

Legend:
Pr(x,t) = eq. (5.5)
P(x,t) = eq. (5.6)

Fig. 5.2. Plot of equations (5.5) and (5.6) for the wave equation with initial triangular distribution.

NOTE: This problem was also solved using the Helmholtz equation. In this case the GFSE used was equation (4.8) together with equation (4.2). During the development of the Green's function it was considered orthonormal functions instead of orthogonal functions to get the constants of the differential equation results. The resulting expression for G was:

$$\boxed{G = \sum_{n=1}^{\infty} \frac{2}{L} \sin\left(\frac{n\pi}{L} x'\right) \sin\left(\frac{n\pi}{L} x\right)} \tag{5.7}$$

After plugging equation (5.7) into equation (4.8) and then into equation (4.2), performing the integrations and further simplification the following result was obtained:

$$p(x,t) = \sum_{n=1}^{\infty} \frac{8\alpha}{(n\pi)^2} \sin\left(\frac{n\pi}{2}\right) \sin\left(\frac{n\pi}{L} x\right) . e^{-i.\frac{n.\pi.c}{L}t} \tag{5.8}$$

Equation (5.8) is also an equivalent expression to equations (5.5) and (5.6). The two approaches of the Green's function technique presented in this work were used to solve the problem and compared with the results found in the literature obtained by the classical separation of variables technique. Final results were exactly the same which validate the technique proposed here. The Helmholtz approach has the advantage of simplicity because it eliminates the time variable in the equation, however this approach may present some difficulties for more complex cases especially when sources are considered. Another advantage of using the wave equation instead of the Helmholtz equation is that the result can be split into the two waves traveling in opposite directions that compose the final result. For example after some algebraic manipulation equation (5.5) can be re-written as:

$$p(x,t)=\sum_{n=1}^{\infty}\frac{4\alpha}{(n\pi)^2}\sin\left(\frac{n\pi}{2}\right)\sin\left(\frac{n\pi}{L}[x-ct]\right)+\sum_{n=1}^{\infty}\frac{4\alpha}{(n\pi)^2}\sin\left(\frac{n\pi}{2}\right)\sin\left(\frac{n\pi}{L}[x+ct]\right) \quad (5.9)$$

In equation (5.9) the first term on the right hand side represents a wave traveling to the right and the second term represents a wave traveling to the left. The advantage of using this presentation is that it allows a reflection coefficient. By including different functions for the reflection coefficient until matching experimental results an accurate reflection coefficient function can be determined.

5.2 ONE-DIMENSIONAL CASE WITH A DISTRIBUTED PERIODIC SOURCE

Consider the one-dimensional non-homogeneous case with the non-homogeneous term given by:

$$F(x) = \sin(\alpha t) \quad (5.10)$$

Similar to the previous case consider homogeneous boundary conditions of the first kind given by $p(0,t) = p(L,t) = 0$ but zero initial conditions (i.e. $p(x,0)=0$ meaning that initially the system is initially undisturbed or at rest).

For this problem the GFSE is also equation (4.13). By applying the boundary and initial conditions all terms on the right hand side of equation (4.13) vanishes except for the last term which contains the source term F. Then the GFSE was reduced to:

$$p(x,t)=\int_0^L\int_0^t GF\,d\tau dx' \quad (5.11)$$

Where F is given by equation (5.10) and the GF comes from equation (4.38). After substitution of these two equations into expression (5.11) the next was obtained:

$$p(x,t)=\int_0^L\int_0^t\sum_{n=1}^{\infty}\frac{-2c}{n\pi}\sin\left(\frac{n\pi}{L}x'\right)\sin\left(\frac{n\pi}{L}x\right)\sin\left(\frac{n\pi c}{L}[t-\tau]\right)\sin(\alpha\tau)d\tau dx' \tag{5.12}$$

An equivalent expression for equation (5.12) is given by equation (5.13) which is easier to integrate:

$$p(x,t)=\sum_{n=1}^{\infty}\frac{-c}{n\pi}\sin(kx)\int_0^L\sin(kx')dx'\left[\sin(kct)\int_0^t[\sin([\alpha+kc]\tau)+\sin([\alpha-kc]\tau)]d\tau-\ldots\right. \tag{5.13}$$

$$\left.-\cos(kct)\int_0^t[\cos([\alpha-kc]\tau)-\cos([\alpha+kc])\tau]d\tau\right.$$

Where: $k=\frac{n\pi}{L}$

After performing the integrations and with the help of trigonometric identities and some algebraic simplifications equation (5.13) was reduced to the following expression:

$$p(x,t)=\sum_{n=1}^{\infty}\frac{2c^2}{n\pi}\frac{\left[(-1)^n-1\right]}{\left[\left(\frac{n\pi c}{L}\right)^2-\alpha^2\right]}\sin\left(\frac{n\pi}{L}x\right)\left(\frac{\alpha L}{n\pi c}\sin\left(\frac{n\pi c}{L}t\right)-\sin(\alpha t)\right) \tag{5.14}$$

A similar problem has also been solved in [53] pp. 754-757. In this reference the authors leave the solution for the constants expressed as integral function of φ(x) where φ(x) is any function to be defined. By considering the factor $1/c^2$ equivalent to g/w in the reference, by making φ(x)=1 and performing the integrations the solution obtained is the same as equation (5.14) as expected.

In the reference the authors assumed the solution to be the superposition of two solutions; one for the homogeneous part and one for the non-homogeneous part. The homogeneous part of the problem was found using the separation of variables technique. For the non-homogeneous part some physical considerations were made together with

half-range sine expansions with known coefficients for the function φ(x) was used to find the solution. The complete solution is the superposition of both the homogeneous and the non-homogeneous parts. Although the source term is distributed in the geometry under study which makes the problem relatively simple notice that the mathematics used in the reference are more involving and the technique more complex than the Green's function technique. This is another advantage of the technique proposed in the present work, its simplicity. Figures (5.3) and (5.4) show some results of equation (5.14)

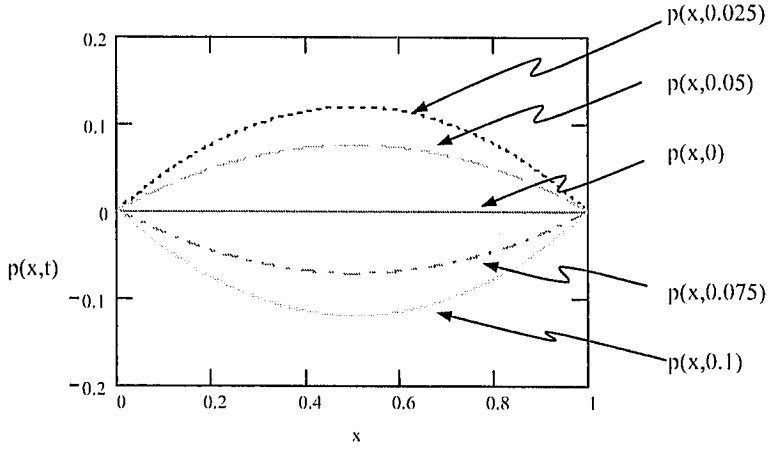

Figure 5.3. Solution at different times for the non-homogeneous wave equation with a distributed periodic source

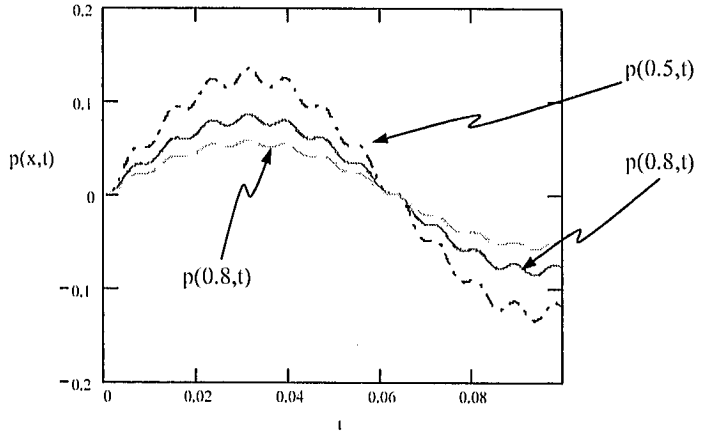

Figure 5.4. Solution at different distances for the non-homogeneous wave equation with a distributed periodic source

5.3. RECTANGULAR MEMBRANE WITH PARABOLIC INITIAL DISTRIBUTION

This 2-D case considers a rectangular membrane with a parabolic initial distribution as indicated below:

$$p(x,y,0) = f(x) = 0.1.(4x - x^2).(2y - y^2) \tag{5.15}$$

The rectangular membrane extends from zero to L in the x direction and from zero to H in the y direction. The boundary conditions are of the first kind in all boundaries and given by:

$$p(0,y,t) = p(L,y,t) = 0 \tag{5.16}$$

$$p(x,0,t) = p(x,H,t) = 0 \tag{5.17}$$

The corresponding GFSE for this 2-D problem is given by equation (4.16) and the GF for this case is given by equation (B.6). Equation (4.16) is recalled below and analyzed term by term:

$$p(x,y,t) = \int_0^t \int_0^H \left\{ \left(p \frac{\partial G}{\partial x'} \right)\Big|_0^L - \left(G \frac{\partial p}{\partial x'} \right)\Big|_0^L \right\} dy' d\tau + \int_0^t \int_0^L \left\{ \left(p \frac{\partial G}{\partial y'} \right)\Big|_0^H - \left(G \frac{\partial p}{\partial y'} \right)\Big|_0^H \right\} dx' d\tau +$$

$$\frac{1}{c^2} \int_0^H \int_0^L \left(\left(p \frac{\partial G}{\partial \tau} \right)\Big|_{\tau=0} - \left(G \frac{\partial p}{\partial \tau} \right)\Big|_{\tau=0} \right) dx' dy' + \int_0^H \int_0^L \int_0^t GF \, d\tau dx' dy'$$

Since all boundary conditions on are homogeneous and of the first kind, the first two double integrals on the right hand side vanish since the terms inside these integrals represent the boundary conditions along axis x and y respectively. In the third integral only the first term remains since it represents the initial condition (given by equation (5.15) for this case). The last term also vanishes since there is not source in this problem. Therefore, after plugging the GF into the simplified GFSE the solution was reduced to:

$$p(x,y,t)=\int_0^H\int_0^L \frac{-0.4}{\pi cLH}\sum_{n=1}^{\infty}\sum_{m=1}^{\infty}\frac{(4x'-x'^2).(2y'-y'^2)}{\sqrt{\left(\frac{n}{L}\right)^2+\left(\frac{m}{H}\right)^2}}\sin(k_1x')\sin(k_2y')\sin(k_1x)\sin(k_2y)\left[\frac{\partial}{\partial\tau}\sin(\omega[t-\tau])\right]_{\tau=0}dx'dy' \tag{5.18}$$

After performing the derivation and integrations as indicated in equation (5.18) and after further simplification the result for this problem was:

$$p(x,y,t)=\frac{0.4}{\pi^2}\sum_{n=1}^{\infty}\sum_{m=1}^{\infty}\frac{1}{mn}\left[(-1)^n\left(-4L+L^2-\frac{2}{k_1^2}\right)+\frac{2}{k_1^2}\right]\left[(-1)^m\left(-2H+H^2-\frac{2}{k_2^2}\right)+\frac{2}{k_2^2}\right]\sin(k_1x)\sin(k_2y)\cos(\omega t) \tag{5.19}$$

Where:

$$\omega=c\sqrt{k_1^2+k_2^2} \tag{5.20a}$$

$$k_1=\frac{n\pi}{L} \tag{5.20b}$$

$$k_2=\frac{m\pi}{H} \tag{5.20c}$$

The solution to this problem can be also found in Kreyszig [52] for the following values to the parameters:

L=4 ; H=2 ; c=5

The solution in the reference has the following presentation:

$$p(x,y,t)=0.42605\sum_{n=odd}^{\infty}\sum_{m=odd}^{\infty}\frac{1}{m^3n^3}\cos\left(\frac{5\pi}{4}\left[\sqrt{m^2+4n^2}\right]t\right)\sin\left(\frac{n\pi}{4}x\right)\sin\left(\frac{m\pi}{2}y\right) \tag{5.21}$$

This is an equivalent expression to that obtained with the use of the Green's function technique for the given values of L, H and c. Figures below show some results.

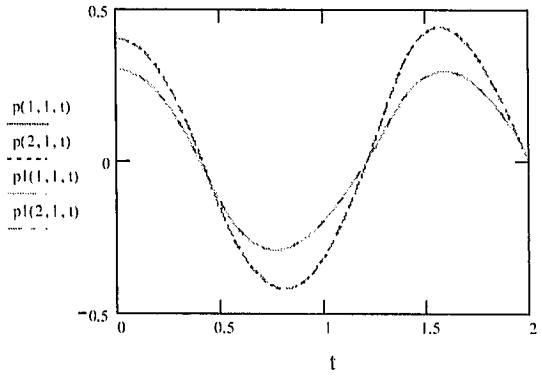

Fig. 5.5a. Equations 5.19 and 5.21 at two different points in the membrane as function of time

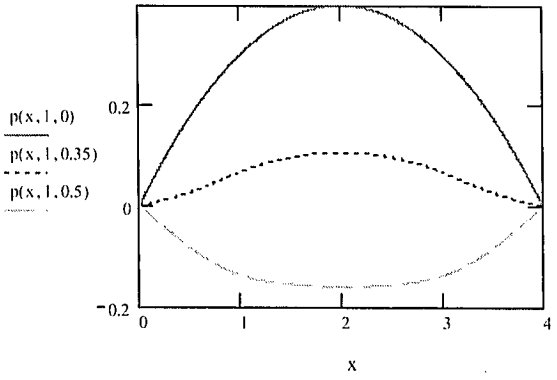

Fig. 5.5b. Eqns. 5.19 and 5.21 along the centerline of the membrane at different times as function of x

Figure (5.5a) shows the membrane displacement as function of time at two different points from both equations (5.19) and equation (5.21). The solutions from both equations superimpose to each other as expected. Figure (5.5b) shows results for the membrane along the centerline at different times along the x axis. Figures (5.6a) through (5.6d) show the surface of the membrane at four different times.

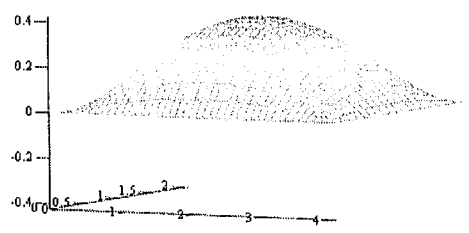

(5.6a)

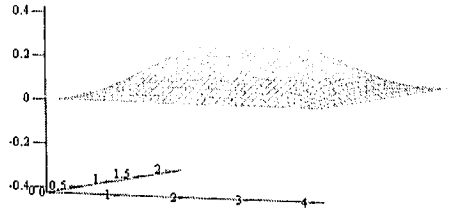

(5.6b)

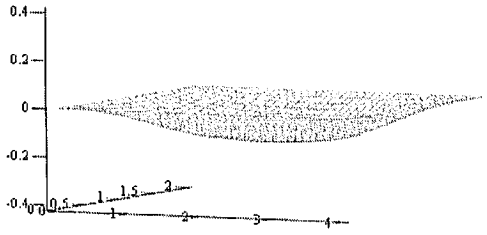

(5.6c)

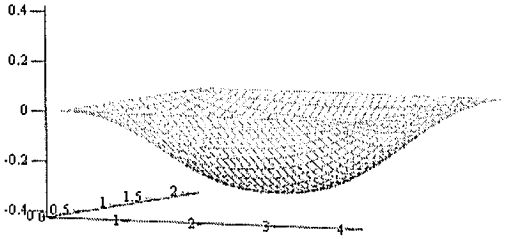

(5.6d)

Fig. 5.6. Membrane displacement

5.4. THIN CIRCULAR MEMBRANE

The previous cases validate the technique proposed in this work for Cartesian coordinates however for the Rijke tube is important to test the technique in cylindrical coordinates. As an example, the next case considers the problem of a circular membrane with an initial distribution given by:

$$p(r,0) = f(r) = 1 - r^2 \tag{5.22}$$

The boundary conditions are of the first kind given by:

$$p(r_0,t) = 0 \tag{5.23a}$$

$$p(0,t) = \text{finite} \tag{5.23b}$$

r_0 is the characteristic radius of the cylinder.

Since this case considers a thin circular membrane it can be considered as a problem with no axial dependence. The GFSE for this cylindrical coordinates for cases with neither axial nor angular dependence is recalled below. Following the same technique the GFSE was determined to be:

$$p(r,t) = \int_0^t r_0 \left\{ \left(p \frac{\partial G}{\partial r'} \right)\Big|_{r'=r_0} - \left(G \frac{\partial p}{\partial r'} \right)\Big|_{r'=r_0} \right\} d\tau + \int_0^{r_0} \left\{ \left(p \frac{\partial G}{\partial \tau} \right)\Big|_{\tau=0} - \left(G \frac{\partial p}{\partial \tau} \right)\Big|_{\tau=0} \right\} + \int_0^t \int_0^{r_0} GF r' dr' d\tau$$

The first term in the first integral in braces is the only term that remains in the right hand side since it represent the initial condition given by equation (5.22). All the other terms vanish. The two terms in the second integral vanish since they represent the boundary conditions given by equations (5.23a) and (5.23b). The last term in double integral also vanishes since it represents the source which is zero for this problem. Therefore the GFSE was reduced to:

$$p(r,z,t)=\frac{1}{c^2}\int_0^{r_0}\left(p\frac{\partial G}{\partial \tau}\right)\Bigg|_{\tau=0} r'dr' \tag{5.24}$$

The corresponding Green's function for this case (recalled below) was found in as:

$$G=\frac{-2c}{r_0^{\,2}}\sum_{m=1}^{\infty}\frac{J_0(k_m r')}{\left[J_1(k_m r)\right]^2.k_m}J_0(k_m r)\sin(\omega[t-\tau])$$

With $\omega = ck_m$

k_m are the zeroes of the eigenfunction $J_0(k_m r_0)=0$

Substitution of the Green's function together with equation (5.22) into equation (5.24) leads to:

$$p(r,z,t)=\int_0^{r_0}\frac{2c^2}{r_0^{\,2}}\sum_{m=1}^{\infty}\frac{J_0(k_m r')}{\left[J_1(k_m r)\right]^2.k_m}J_0(k_m r)\cos(\omega.t).(1-r'^2)r'dr' \tag{5.25}$$

After performing the integrations taking into account the properties of the Bessel functions, the following result was obtained:

$$p(x,t)=\frac{2}{r_0}\sum_{m=1}^{\infty}\frac{J_0(k_m r).\cos(k_m ct)}{\left[J_1(k_m r_0)\right]^2.k_m}\left[J_1(k_m r_0)\left(1-r_0^{\,2}+\frac{4}{k_m^{\,2}}\right)-\frac{2r_0}{k_m}J_0(k_m r_0)\right]$$

Since $J_0(k_m r_0) = 0$ by condition of the eigenfunction, then the final result was obtained as:

$$p(r,t)=\frac{2}{r_0}\sum_{m=1}^{\infty}\frac{J_0(k_m r).\cos(k_m ct)}{J_1(k_m r_0).k_m}\left(1-r_0^{\,2}+\frac{4}{k_m^{\,2}}\right) \tag{5.26}$$

The solution to this problem can also be found in Kreiszig [52] for $r_0=1$ and $c=2$. The solution given by the author has the following presentation:

$$p(r,t) = 1.1018 J_0(2.4048 r).\cos(4.8097 t) - 0.140 J_0(5.5021 r).\cos(11.0402 t) + 0.045 J_0(8.6537 r).\cos(17.3075 t) - \ldots \quad (5.27)$$

Equations (5.26) and (5.27) were plotted to show the membrane displacement at times 0.35 seconds, 0.2 seconds and zero seconds to show the initial distribution. Results are shown in figure (5.7) below. Notice plots from both equations (5.26) and (5.27) are exactly the same and lines superimpose to each other. Figures (5.8a) through (5.8d) show the surface of the membrane at four different times.

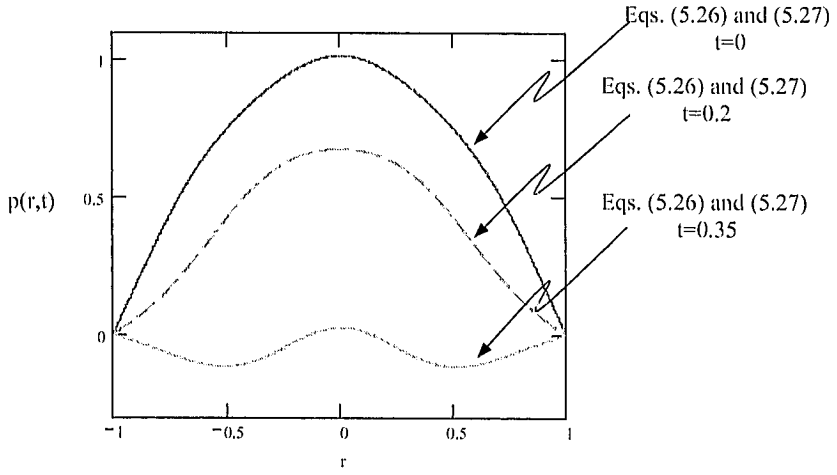

Fig. 5.7 Membrane displacement. Equations (5.26) and (5.27) at times 0, 0.2 and 0.35 seconds

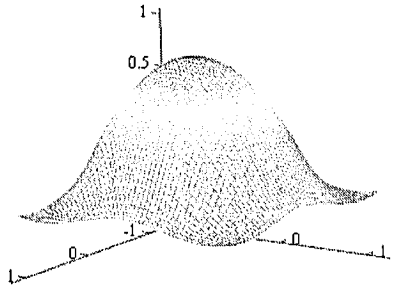

Fig. 5.8a.

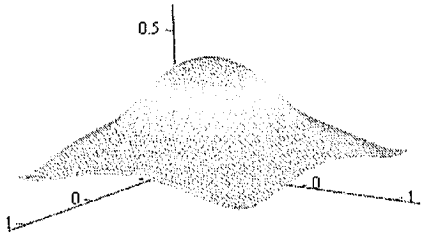

Fig. 5.8b

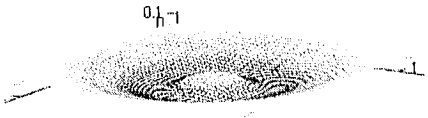

Fig. 5.8c

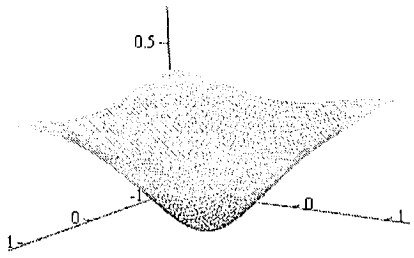

Fig. 5.8d

Fig. 5.8. Membrane displacement, surface plot

5.5. VARIABLE SPEED OF SOUND

In this part of the present work a case of variable speed of sound is analyzed. It was considered a one dimensional problem with parabolic temperature profile as shown in figure 5.9. This problem was already considered in page 42 where a general solution for any kind of boundary conditions was found and then boundary conditions of first kind were applied to arrive to a final solution.

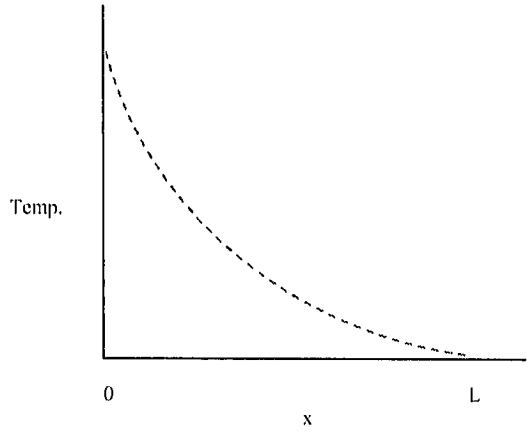

Fig. 5.9. Parabolic temperature profile

Now, the case where one boundary condition is of first kind and the other of second kind is considered. A similar problem was solved by Sujith et al. [54]. In their

work they solved the 1-D acoustic field for a length L=4m and a linear temperature profile for several values of the slope. They kept fixed the temperature at the exit at 300K and the values of the temperature at the entrance were 300K, 500K, 700K, 900K and 1100K. The parabolic temperature profile (Tp) of the present work (given by equation (4.44)) was carefully chosen such that it closely matches the linear temperature profile (Tl) of Sujith's work. Notice the similitude of both the linear and parabolic temperature profiles shown in Figure 5.10.

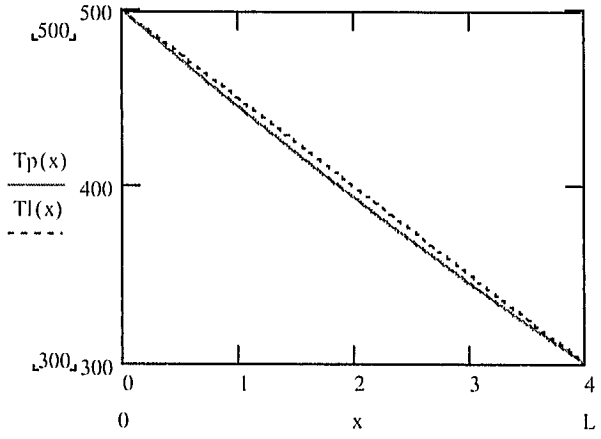

Fig. 5.10. Parabolic and linear temperature profiles

In their study Sujith et al. considered the boundary conditions given by:

$$\left.\frac{\partial p}{\partial x}\right|_{x=0} = 0 \tag{5.28a}$$

$$p(L,t) = 0 \tag{5.28b}$$

From the separation of variables technique it was assumed that the complete solution of the problem is the product of two functions of a single variable given by equation (4.41). Therefore the boundary conditions can be rewritten as:

$$\left.\frac{dX}{dx}\right|_{x=0} = 0 \tag{5.29a}$$

$$X(L) = 0 \tag{5.29b}$$

Similarly to the case analyzed previously in section 4.4.2, the three possible solutions given by equations (4.54a), (4.54b) and (4.54c) were analyzed for the boundary conditions given by equations (5.29a) and (5.29b) and the parameters used by Sujith et al. in their work:

CASE I: D = 0

Equation (4.54.a) is the mathematical solution for case of D=0. This is not a physical possible solution for the problem because when it comes to satisfy the boundary conditions the solution fails. For the boundary condition (5.29a), the following was obtained:

$$\left[-\frac{A}{2}\frac{b}{\sqrt{(|b.x+1|)^3}} + B\frac{1}{\sqrt{(|b.x+1|)^3}} - \frac{B}{2}\frac{\ln(|b.x+1|)}{\sqrt{(|b.x+1|)^3}}\right]_{x=0} = 0 \tag{5.30}$$

Therefore:

$$B = A.b/2 \tag{5.31}$$

With equation (5.31) and the boundary condition (5.29b) plugged into (4.54a), the following was found:

$$Ln|b.L+1| = -2 \tag{5.32}$$

If the case of temperature varying from 500K to 300K is considered, then the only possible value of the length L that satisfies the eigenfunction equation (5.32) would be a

negative number (-15.344m) which is not physically possible. On the other hand, if L=4m is chosen, then equation (5.32) is not satisfied.

CASE II: D>0

The mathematical solution for this case is given by equation (4.54b). Considering boundary condition (5.29a), the following expression was obtained:

$$\frac{-A}{\sqrt{(|b.x+1|)^3}}\left[-\frac{b}{2}.\sinh\left(\frac{1}{2b}\sqrt{\left\{b^2-4\frac{\omega^2}{\xi}\right\}}\ln|b.x+1|\right)+\frac{1}{2}\sqrt{\left\{b^2-4\frac{\omega^2}{\xi}\right\}}\cosh\left(\frac{1}{2b}\sqrt{\left\{b^2-4\frac{\omega^2}{\xi}\right\}}\ln|b.x+1|\right)\right]_{x=0}+$$

$$\frac{-B}{\sqrt{(|b.x+1|)^3}}\left[-\frac{b}{2}.\cosh\left(\frac{1}{2b}\sqrt{\left\{b^2-4\frac{\omega^2}{\xi}\right\}}\ln|b.x+1|\right)+\frac{1}{2}\sqrt{\left\{b^2-4\frac{\omega^2}{\xi}\right\}}\sinh\left(\frac{1}{2b}\sqrt{\left\{b^2-4\frac{\omega^2}{\xi}\right\}}\ln|b.x+1|\right)\right]_{x=0}=0$$

After simplification it was found:

$$B=\frac{A}{b}\sqrt{b^2-4\frac{\omega^2}{\xi}} \tag{5.33}$$

By substitution of equation (5.33) and boundary condition (5.29b) into (4.54.b) the next expression was found:

$$\frac{A}{\sqrt{b.L+1}}\left[\sinh\left(\frac{1}{2b}\sqrt{\left\{b^2-4\frac{\omega^2}{\xi}\right\}}\ln|b.L+1|\right)+\frac{1}{b}\sqrt{\left\{b^2-4\frac{\omega^2}{\xi}\right\}}\cosh\left(\frac{1}{2b}\sqrt{\left\{b^2-4\frac{\omega^2}{\xi}\right\}}\ln|b.L+1|\right)\right]=0$$

After some simplification this expression becomes:

$$\tanh\left(\frac{1}{2b}\sqrt{\left\{b^2-4\frac{\omega^2}{\xi}\right\}}\ln|b.L+1|\right)+\frac{1}{b}\sqrt{\left\{b^2-4\frac{\omega^2}{\xi}\right\}}=0$$

Or:

$$\tanh\left(\frac{1}{2b}\sqrt{D}\ln|b.L+1|\right)+\frac{1}{b}\sqrt{D}=0 \tag{5.34}$$

This last equation is satisfied only if D=0 which is contrary to the initial assumption of D>0.

CASE III: D<0

Following the procedure as in the two previous cases, after substitution of the boundary conditions the eigenfunction was found to be:

$$\tan\left(\frac{1}{2b}\sqrt{\left\{4\frac{\omega^2}{\xi}-b^2\right\}}\ln|b.L+1|\right)+\frac{1}{b}\sqrt{\left\{4\frac{\omega^2}{\xi}-b^2\right\}}=0 \tag{5.35}$$

The characteristic frequencies (ω) were found by determining the zeroes of equation (5.35) and then solving for ω. The values of the first five frequencies for a temperature profile varying from 500K to 300K are shown in table 5.1 and compare with the results from Sujith [54].

Temperature Profile	First (Hz)	Second (Hz)	Third (Hz)	Fourth (Hz)	Fifth (Hz)
Linear [54]	23.61	74.23	124.15	173.97	223.77
Parabolic	23.408	73.625	123.142	172.594	221.976

Table . 5.1. Characteristic frequencies for the linear and parabolic temperature profiles

The values of the frequencies are not expected to be the same since they come from different temperature profiles however; they have to be close since the profiles were chosen such that the linear and parabolic profiles were very similar (see. Fig. 5.10). Same behavior was found for temperature profiles with different slopes also shown in Sujith's paper [54].

5.6. VALIDATION WITH EXPERIMENTAL RESULTS: SIDE BRANCH PIPE

All the previous cases helped to validate the Green's functions technique. Those relatively simple problems were solved using the Green's functions technique and compared with the solutions found in the literature. Now the technique is tested with actual data by solving the problem of a side branch pipe. The experimental setup for this case is shown in figure 5.11. The experimental setup and the data were kindly supplied by Douglas Straub from NETL.

The speaker acted as an acoustic source that sent a sinusoidal signal of known frequency α to the system. The response of the system was measure at P1 and P2. The different values given to α were 200Hz, 300Hz and 400Hz.

Because of the geometrical configuration of the piping this is a 3-D cylindrical problem. Therefore a 3-D GFSE for cylindrical coordinates was developed by following the same procedure as the one used to arrive to equation (4.19) but this time variations in the azimuthal direction were included.

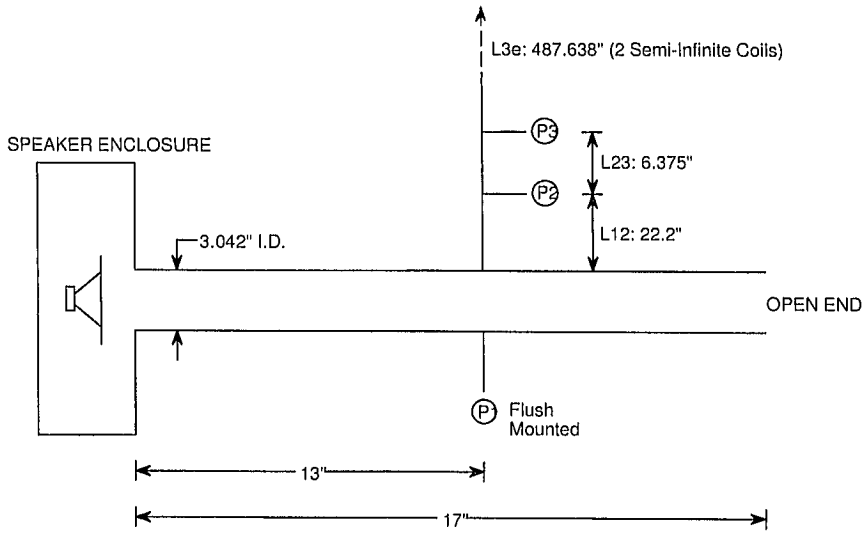

Fig. 5.11. Experimental set up for the side branch pipe (courtesy of Douglas Straub-NETL)

The non-homogeneous 3-D wave equation in cylindrical and its corresponding auxiliary equation are given by:

$$\frac{1}{r}\frac{\partial}{\partial r}\left(r\frac{\partial p}{\partial r}\right)+\frac{1}{r^2}\frac{\partial^2 p}{\partial \theta^2}+\frac{\partial^2 p}{\partial z^2}-\frac{1}{c^2}\frac{\partial^2 p}{\partial t^2}=F \tag{5.36}$$

$$\frac{1}{r}\frac{\partial}{\partial r}\left(r\frac{\partial G}{\partial r}\right)+\frac{1}{r^2}\frac{\partial^2 G}{\partial \theta^2}+\frac{\partial^2 G}{\partial z^2}-\frac{1}{c^2}\frac{\partial^2 G}{\partial t^2}=\delta(\vec{r}-\vec{r}')\delta(t-\tau) \tag{5.37}$$

The spatial part of the Dirac-delta function in equation (5.37) was written as $\delta(\vec{r}-\vec{r}')$ for simplicity however, the actual Dirac-delta function for cylindrical coordinates is given by:

$$\frac{1}{\pi . r}\delta(r-r')\delta(\theta-\theta')\delta(z-z') \tag{5.38}$$

Integration of the Dirac-delta function gives one as result (see properties of the Dirac-delta function in section 3.2.1)

Multiplying equation (5.36) by G, equation (5.37) by p, subtracting the results from each other and applying integrations in r,θ,z and τ, the following was obtained:

$$\int_0^t\int_0^{2\pi}\int_0^L\int_0^{r_0} p(r,z,\theta,t).\delta(\vec{r}-\vec{r}')\delta(t-\tau).r'dr'dz'd\theta'.d\tau = \int_0^t\int_0^{2\pi}\int_0^L\int_0^{r_0}\left\{\frac{p}{r'}\frac{\partial}{\partial r'}\left(r'\frac{\partial G}{\partial r}\right)-\frac{G}{r'}\frac{\partial}{\partial r'}\left(r'\frac{\partial p}{\partial r'}\right)+\right.$$

$$\left.\frac{p}{r'^2}\frac{\partial^2 G}{\partial\theta'^2}-\frac{G}{r'^2}\frac{\partial^2 p}{\partial\theta'^2}+p\frac{\partial^2 G}{\partial z'^2}-G\frac{\partial^2 p}{\partial z'^2}-\frac{p}{c^2}\frac{\partial^2 G}{\partial\tau'^2}+\frac{G}{c^2}\frac{\partial^2 p}{\partial\tau'^2}+G.F\right\}r'dr'dz'd\theta'd\tau$$

(5.39)

Applying properties of Dirac-delta function to the left hand side, performing integrations by parts to all the terms on the right hand side and some further simplifications, the following was obtained:

$$p=\int_0^t\int_0^{2\pi}\int_0^L r_0\left\{\left(p\frac{\partial G}{\partial r'}\right)\Big|_{r_0}-\left(G\frac{\partial p}{\partial r'}\right)\Big|_{r_0}\right\}dz'd\theta'd\tau+\int_0^t\int_0^{r_0}\int_0^L\frac{1}{r'}\left\{\left(p\frac{\partial G}{\partial\theta'}\right)\Big|_0^{2\pi}-\left(G\frac{\partial p}{\partial\theta'}\right)\Big|_0^{2\pi}\right\}dz'dr'd\tau+$$

$$\int_0^t\int_0^{2\pi}\int_0^{r_0} r'\left\{\left(p\frac{\partial G}{\partial z'}\right)\Big|_0^L-\left(G\frac{\partial p}{\partial z'}\right)\Big|_0^L\right\}dr'd\theta'd\tau+\int_0^{r_0}\int_0^{2\pi}\int_0^L\frac{r'}{c^2}\left\{\left(G\frac{\partial p}{\partial\tau}\right)\Big|_{\tau=0}-\left(p\frac{\partial G}{\partial\tau}\right)\Big|_{\tau-0}\right\}dz'd\theta'dr'+$$

$$\int_0^\tau\int_0^{2\pi}\int_0^L\int_0^{r_0} GFr'dr'dz'd\theta'd\tau$$

(5.40)

Equation (5.40) is the 3-D GFSE for cylindrical coordinates. The terms in the three first triple integrals accounts for the boundary conditions in r, θ and z directions respectively. The terms in the fourth triple integral account for the initial conditions and the last term in the quadruple integral accounts for the source.

For the analytical model of the side branch pipe the speaker was considered as a source of strength Λ at the entrance of the pipe. Also a sink of strength Λ_1 was considered

where the side branch is placed. The source and sink are shown in figure 5.12. Applying equation (5.40) to the case of the side branch pipe all terms but the source vanishes resulting in the following expression:

$$p(r,\theta,z,t) = \int_0^t \int_0^{2\pi} \int_0^L \int_0^R GFr'\,dr'\,dz'\,d\theta'\,d\tau \tag{5.41}$$

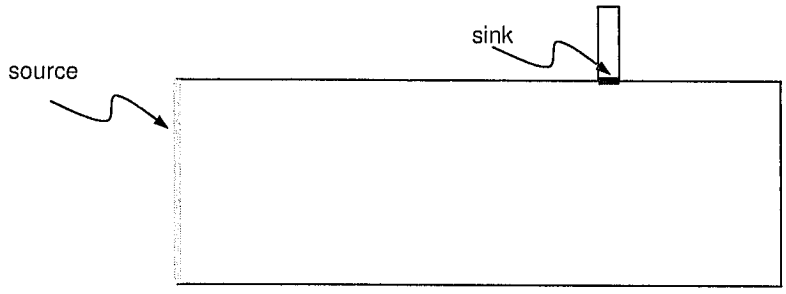

Fig. 5.12. Source and sink considered for the analytical model of the side branch pipe.

The complete solution can be considered as the summation of two separate solutions, one for the source and one for the sink. The boundary conditions were:

$$p(r,\theta,0,t) = 0 \tag{5.42a}$$

$$p(r,\theta,L,t) = 0 \tag{5.42b}$$

$$\left.\frac{\partial p}{\partial r}\right|_{r=r0} = 0 \tag{5.42c}$$

$$p(0,\theta,z,t) = \text{finite real number} \tag{5.42d}$$

The GF function for this case, which is presented next, was obtained by finding the solution for a pipe with boundary conditions (5.42a) through (5.42d) and initial condition $p(r,\theta,z,0) = F$ where $F = F(r,\theta,z)$.

$$G = \sum_{n}^{\infty}\sum_{m}^{\infty}\sum_{\nu}^{\infty} \frac{2c}{\pi} \frac{\sin(\nu\theta').\sin(k_1 z').J_\nu(\lambda_m r')}{k.\left[\int_0^{r0} rJ_\nu(\lambda_m r)dr\right]^2} \sin(\nu\theta).\sin(k_1 z).J_\nu(\lambda_m r).\sin(k.c.[t-\tau])$$

(5.43)

Were k_1, k and λ_m are defined as follows:

$$k_1 = \frac{n\pi}{L} \tag{5.44a}$$

$$J_n(\lambda_m r_0) - \left(\frac{n+1}{\lambda_m r_0}\right).J_{n+1}(\lambda_m r_0) = 0 \tag{5.44b}$$

$$k = \sqrt{(k_1)^2 + (\lambda_m)^2} \tag{5.44c}$$

The source was assumed to be at a distance "a" from the entrance and applied to the whole cross sectional area of the pipe. The value of "a" was chosen to be a very small number such that a→0. The source was expressed mathematically as:

$$F = \Lambda.\sin(\alpha.\tau).\delta(x'-a) \tag{5.45}$$

Where:

Λ is the strength of the source,

α is the frequency of the source in rad/s

Equation (5.45) guarantees that the source is a sinusoidal signal of strength Λ and is acting only at the entrance of the pipe.

The mathematical expression for the sink was:

$$f = \Lambda_1.\sin(\alpha.\tau)\delta(r'-r_0)[H(z'-a_1) - H(z'-a_2)][H(\theta-\theta 1) - H(\theta-\theta 2)] \tag{5.46}$$

H is the step function

Λ_1 is the strength of the sink.

Equation (5.46) guarantees that the sink is acting only at the area were the side pipe is placed.

Solutions were found for the source and sink separately by substituting equations (5.43) and (5.45) into (5.41) for the source; and equations (5.43) and (5.46) into (5.41) for the sink. The expressions obtained are presented in the next page. Notice that the solutions can be easily separated into two waves, one wave traveling to the right and the other wave traveling to the left. In this way the reflected wave can be adjusted to match the experimental data, in this manner the amount of energy reflected at the boundaries can be accounted. Accurate account of the reflection coefficient may help to predict the onset of combustion instabilities. Figures (5.13), (5.14) and (5.15) show some results from the analytical analysis and from the experimental data for different values of input frequencies.

The complete solution for the analytical analysis was given by:

$$p(r,\theta,z,t) = p_{sc}(z,t) + p_{sk1}(z,t) + p_{sk2}(r,\theta,z,t) \tag{5.47}$$

Since the complete expressions for equations $p_{sc}(z,t)$, $p_{sk1}(z,t)$ and $p_{sk2}(r,\theta,z,t)$ are very long they are shown in the next page by equations (5.48), (5.49) and (5.50).

Solution for the source:

$$p_{Sc}(z,t)=\sum_{n=1}^{\infty}\frac{4.c.\Lambda}{n.\pi}\frac{\sin\left(\frac{n\pi}{L}a\right)}{\left[\left(\frac{n\pi}{L}c\right)^2-\alpha^2\right]}\sin\left(\frac{n\pi}{L}z\right).\left[\alpha.\sin\left(\frac{n\pi}{L}c.t\right)-\frac{n\pi}{L}c.\sin(\alpha.t)\right] \tag{5.48}$$

For the sink the following expressions were found:

$$p_{sk1}(z,t)=\frac{2.c.\Lambda_1.L.(\theta_2-\theta_1)}{r_0.\pi^2}\sum_{n}^{\infty}\frac{\left(\cos\left(\frac{n.\pi}{L}a_2\right)-\cos\left(\frac{n.\pi}{L}a_1\right)\right)}{(n.\pi)^2.\left[\left(\frac{n.\pi.c}{L}\right)^2-\alpha^2\right]}\sin\left(\frac{n.\pi}{L}z\right).\left[.\frac{n.\pi}{L}c.\sin(\alpha.t)-\alpha.\sin\left[\frac{n.\pi}{L}c.t\right]\right] \quad (\nu=0) \tag{5.49}$$

$$p_{sk2}(r,\theta,z,t)=\frac{4.c.\Lambda}{r_0.\pi}\sum_{n}^{\infty}\sum_{m}^{\infty}\sum_{\nu}^{\infty}\frac{[\cos(\nu.\theta_2)-\cos(\nu.\theta_1)]\left\{\cos\left(\frac{n.\pi}{L}a_2\right)-\cos\left(\frac{n.\pi}{L}a_1\right)\right\}}{n.\pi.k.\sqrt{\left(\frac{n.\pi}{L}c\right)^2-\alpha^2}}J_\nu(k_m r_0).\sin(\nu.\theta).\sin\left(\frac{n.\pi}{L}z\right).J_\nu(k_m.r).[k.c.\sin(\alpha.t)-\alpha.\sin(k.c.t)] \quad (\nu\neq 0) \tag{5.50}$$

Were:

$$k=\sqrt{\left(\frac{n.\pi}{L}\right)^2+(k_m)^2}$$

The first term on the right hand side in equation (5.47) $p_{sc}(z,t)$ is the solution for the source. Notice that $p_{sc}(z,t)$ automatically came one dimensional. The pressure varies only in the axial direction. This was expected since the source was uniformly applied over the whole cross sectional area of the pipe.

The second and third terms together are the solution for the sink. Since the problem is in cylindrical coordinates, the solutions are expected to come in terms of the Bessel functions. $P_{sk1}(z,t)$ is the part of the solution for $\nu = 0$ in the Bessel equation.

Experimental and model results are shown in figures 5.13 through 5.15 for source frequencies of 200Hz, 300Hz and 400Hz respectively. Notice that the results are in good agreement with the experimental data. The frequency spectrum of the experimental data was obtained by applying the Fourier transformation to the collected data. As for the analytical model the frequency spectrum was found by applying the Fourier transformation to the values calculated by the model. These values were obtained at the same intervals of time as the experimental data was collected. In this case the data was collected at a rate of 3000 data per second.

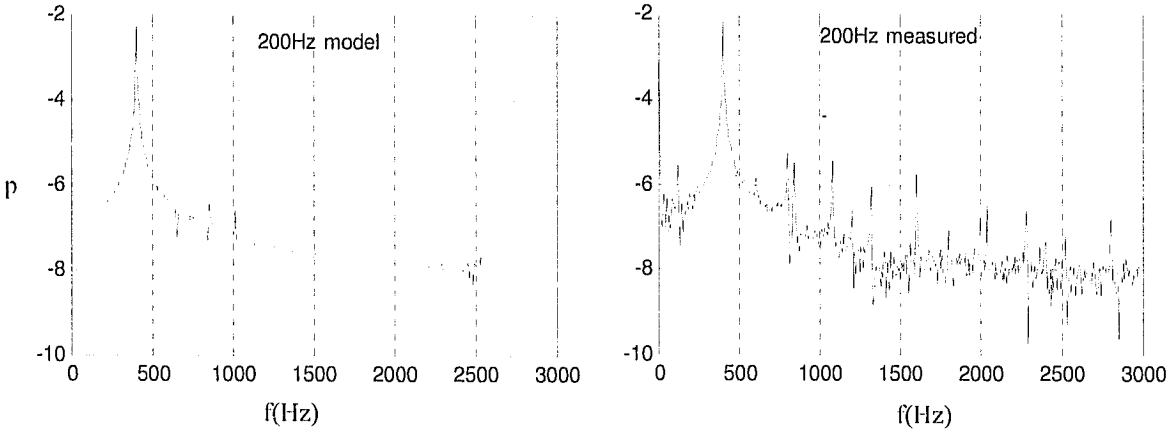

Fig. 5.13. Measured and calculated power spectrum for an input of 200Hz.

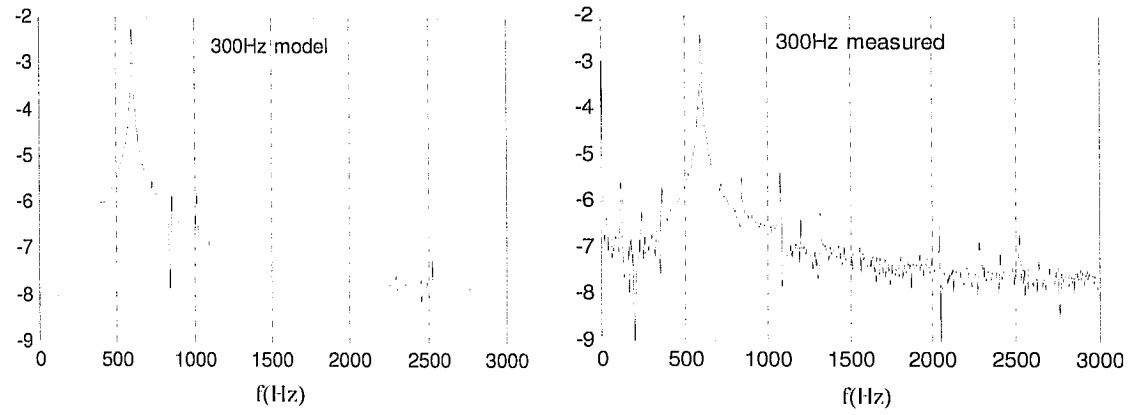

Fig. 5.14 Measured and calculated power spectrum for an input of 300Hz.

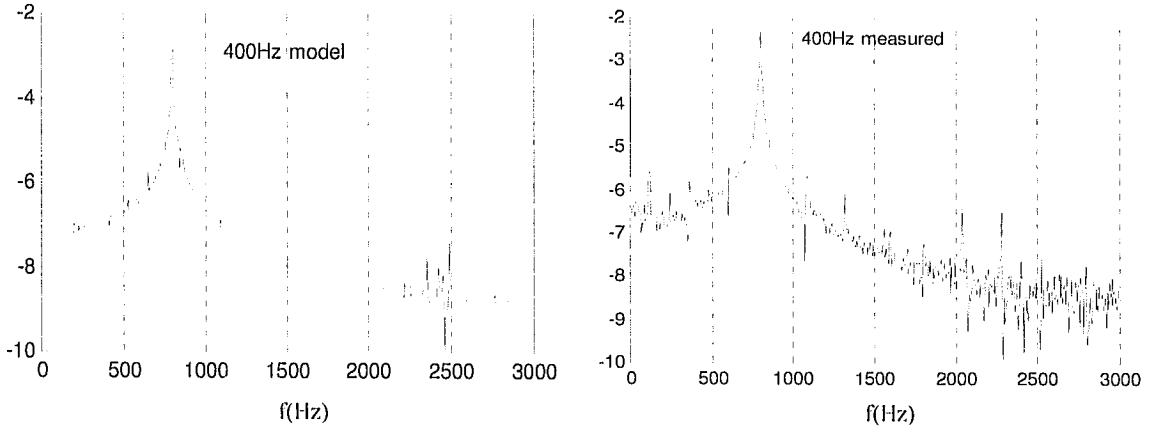

Fig. 5.15. Measured and calculated power spectrum for an input of 400Hz.

The agreement between the experimental data with analytical model validates the technique proposed in this work. Figures 5.16a through 5.16d show some snapshots of the pressure distribution obtained from the analytical model at the neighborhood of the side branch pipe.

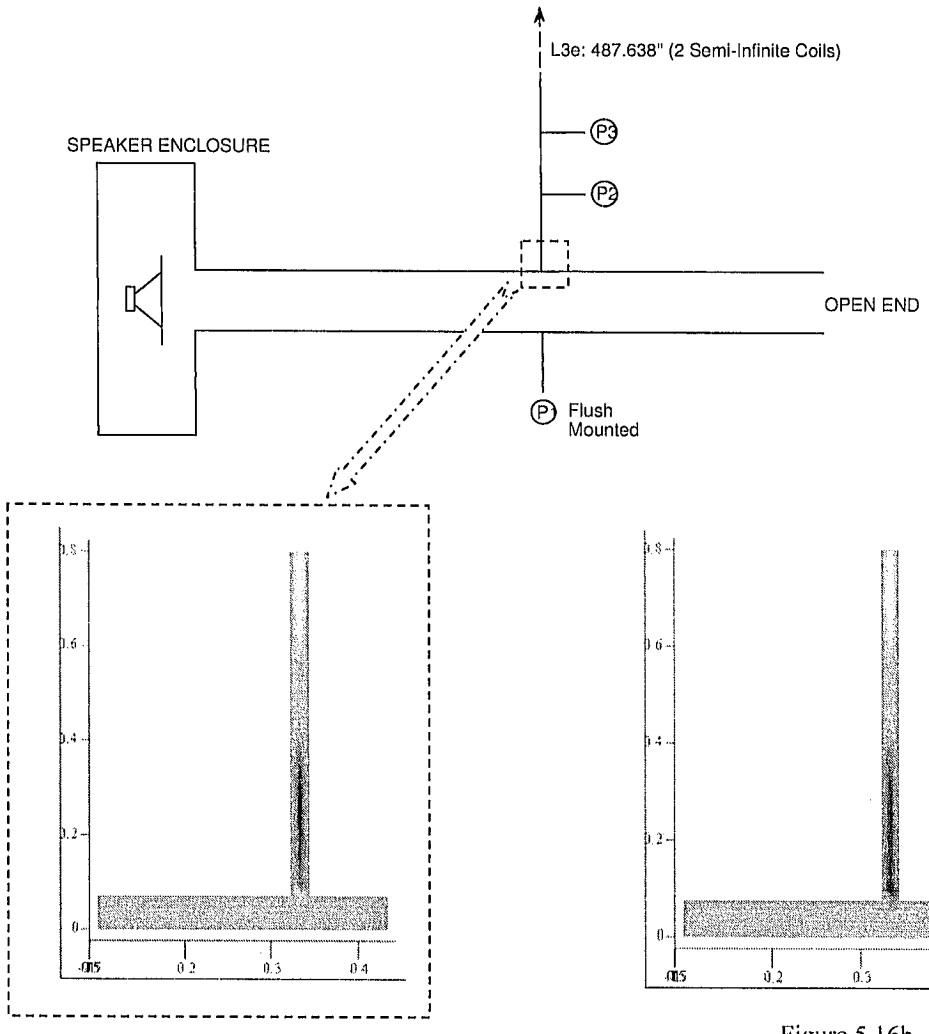

Figure 5.16a

Figure 5.16b

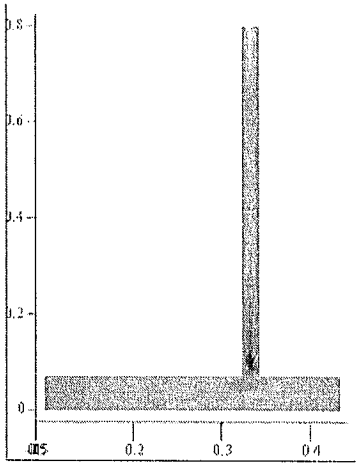

Figure 5.16c

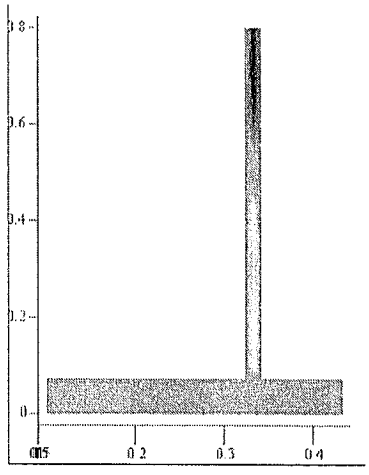

Figure 5.16d

Figures 5.16a - 5.16d.- Pressure distribution at the neighborhood of the side branch pipe.

5.7. THE RIJKE TUBE MODEL

Figure (4.1b) in section 4.1 showed the regions the Rijke tube was divided into in order to apply the technique proposed in this study. Regions I and II are the most important since this regions contributes the most to the pressure distribution.

For example consider a periodic source of strength Λ placed at the entrance of region I. This is similar to the case of the sided branch pipe considering only the source. The solution was already presented in section 5.6. In this case the solution was given by:

$$p_I(x,t)=\sum_{n=1}^{\infty}\frac{-4.c.\Lambda}{n.\pi}\frac{\sin\left(\frac{n\pi}{L}a\right)}{\left[\left(\frac{n\pi}{L}c\right)^2-\alpha^2\right]}\sin\left(\frac{n\pi}{L}x\right).\left[\alpha.\sin\left(\frac{n\pi}{L}c.t\right)-\frac{n\pi}{L}c.\sin(\alpha.t)\right] \qquad (5.51)$$

Note: the solution started from the 2-D GFSE but automatically the solution became 1-D. This is expected since the source was applied over the whole area of the entrance.

For region II the solution was obtained from the combination of a 2-D approach with constant speed of sound together with a 1-D with variable speed of sound approach. For the 2-D approach the following expression was obtained:

$$p_{IIC}(x,r,t)=\sum_{n=1}^{\infty}\frac{-2..\Lambda.c.r_0^2}{n.\pi.r_1^2}\sin\left(\frac{n.\pi}{L_1}.L_0\right).\sin\left(\frac{n.\pi}{L_1}.[x-L_2]\right)\frac{1}{\left(\left(\frac{n.\pi}{L_1}c\right)^2-\alpha^2\right)}.\left(\frac{n.\pi}{L_1}.c.\sin(\alpha.t)-\alpha.\sin\left(\frac{n.\pi}{L_1}.c.t\right)\right)+$$

$$\sum_{n=1}^{\infty}\sum_{m=1}^{\infty}\frac{-4.c.\Lambda..J_1(\beta_m.r_0)}{\beta_m.n.\pi.r_1^2\left[J_0(\beta_m.r_1)\right]^2}\sin\left(\frac{n.\pi}{L_1}L_0\right).\sin\left(\frac{n.\pi}{L_1}[x-L_2]\right).J_0(\beta_m.r).\frac{[k.c.\sin(\alpha.t)-\alpha.\sin(k.c.t)]}{(k.c)^2-\alpha^2} \qquad (5.52)$$

Where k is given by the following expression:

$$k = \sqrt{\left(\frac{n.\pi}{L_1}\right)^2 + \beta_m^2} \tag{5.53}$$

The values of β_m are the zeroes of the equation below:

$$J_1(\beta_m . r_1) = 0 \tag{5.54}$$

The zeroes of equation (5.54) give ($\beta_m . r_1$), from there the value of β_m can be easily obtained since r_1 is known (see figure 5.17 for dimensions of r0, r1 and the complete configuration).

The 1-D variable speed of sound approach resulted in equation (5.56) shown in next page.

The angular frequency ω of equation (5.56) is given by the following equation:

$$\omega = \frac{1}{2}\sqrt{\gamma.R.a.\left[\left(\frac{2.n.\pi.b}{\ln(|b.L_1 + 1|)}\right)^2 + b^2\right]} \tag{5.55}$$

The values of the constants a and b depend on the maximum and minimum temperatures chosen for the parabolic profile given by equation (4.44).

If the parabolic profile is chosen the same as the shown in figure 5.10 where the maximum temperature is 500 K and the minimum 300 K, then the first characteristic frequency obtained from equation (5.55) is ω = 247 Hz for the dimensions of the Rijke tube considered in this work (see figure 5.17). NOTE: the value obtained from equation (5.55) is actually given in rad/s then it was converted to Hz.

Equations (5.52) and (5.56) summarize the solution for regions I and II of the Rijke tube when a 200Hz sinusoidal source is considered.

$$p_{III}(x,t) = \sum_{n=1}^{\infty} \frac{2.\omega.b}{\ln\left(\left|b.L_1 + 1\right|\right)} . \frac{1}{\sqrt{\left|b.L_0 + 1\right|}} . \sin\left[\frac{1}{2.b}\sqrt{-D}.\ln\left(\left|b.L_0 + 1\right|\right)\right] . \frac{1}{\sqrt{\left|b.x + 1\right|}} . \sin\left[\frac{1}{2.b}\sqrt{-D}.\ln\left(\left|b.x + 1\right|\right)\right] . \frac{1}{\omega^2 - \alpha^2}\left[\omega.\sin(\alpha.t) - \alpha.\sin(\omega.t)\right] \tag{5.56}$$

$$D = \sqrt{b^2 - \frac{4.\omega^2}{\gamma.R.a}} \tag{5.57}$$

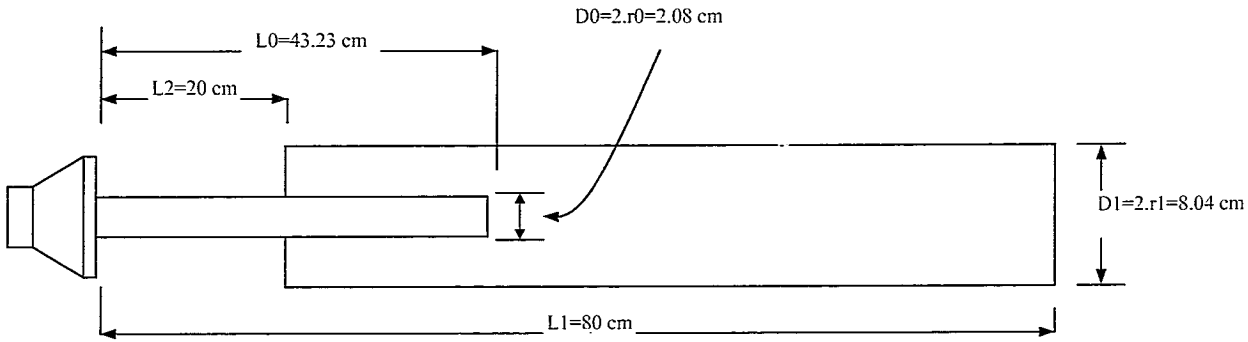

Fig. 5.17. Rijke tube configuration (Ferguson [49])

Figures 5.18 a through d show snapshots of the 2-D solution with constant speed of sound obtained from a contour plot of equation (5.52). Figures 5.19 a through d show snapshots of the 1-D solution with variable speed of sound obtained from equation (5.56); figures 5.20 a through d show snapshots for a combination of equations (5.52) and (5.56)

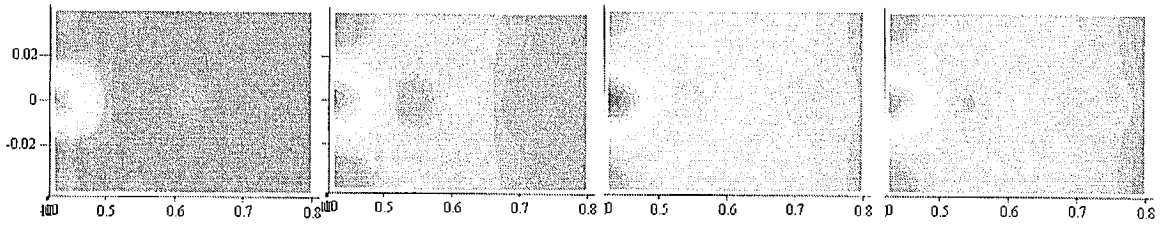

Fig. 5.18. Two-dimensional pressure distribution for constant speed of sound

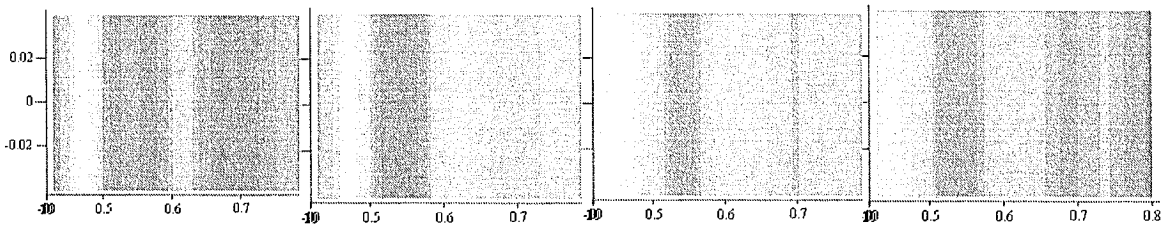

Fig. 5.19. One-dimensional pressure distribution for variable speed of sound

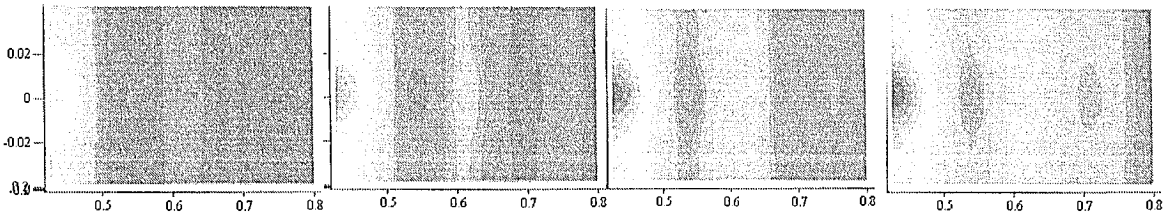

Fig. 5.20. Pressure distribution for combination of 2-D with constant speed of sound and 1-D variable speed of sound

Figures 5.21, 5.22 and 5.23 are the Fourier transform (FT) of the numerical results obtained from equations (5.52) and (5.56). Figure 5.21 shows the FT for region II when only a 2-D pressure distribution with constant speed of sound was considered. Figure 5.22 shows the FT when only a 1-D pressure distribution with axially variable speed of sound was considered. Finally, figure 5.23 shows the FT when the pressure distribution was considered as a combination of the two previous cases. Notice that several harmonics were triggered for the variable speed of sound. NOTE: the data was collected at a point close to the end of the small pipe (at x = 44 cm)

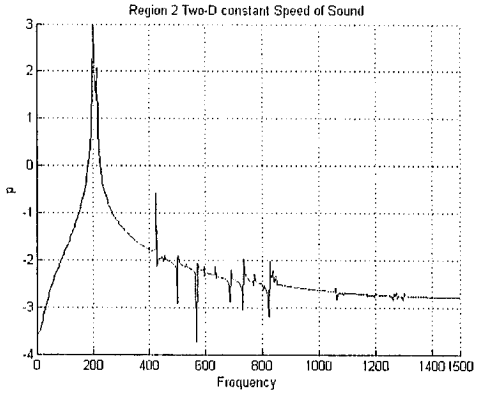

Fig. 5.21. FT for the 2-D pressure distribution with constant speed of sound

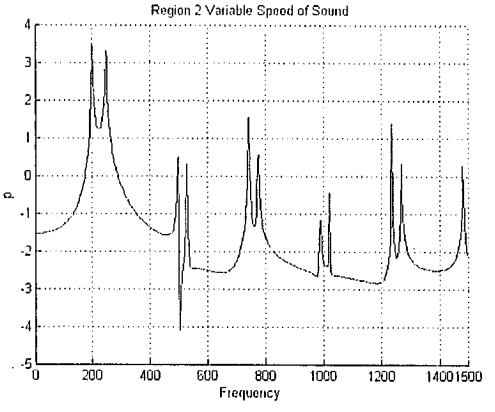

Fig. 5.22. FT for the 1-D pressure distribution with variable speed of sound

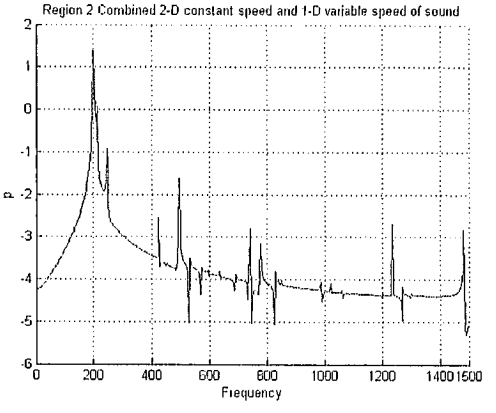

Fig. 5.23. FT for the combined 2-D pressure distribution with constant speed of sound and 1-D pressure distribution with variable speed

CHAPTER VI

CONCLUSIONS AND FUTURE WORK

6.1. CONCLUSIONS

A technique using the Green's Functions for solving the wave equation was introduced in this work. This technique allows solving problems whether acoustic sources (or sinks) are present or not. If sources are present these can be distributed or discrete. The results found using this technique were compared with results found in literature showing to be in good agreement. One and two-dimensional problems with constant speed of sound and a one-dimensional model with axially variable speed of sound were considered. In addition a 3-D model for a side branch pipe was considered and the results showed to be in good agreement with the experimental data. The solutions were closed form mathematical expressions which facilitate the tabulation of numerical results and eases the plotting in any mathematical software such as MatCad, MatLab even Excel. On the other hand, if finite differences techniques are used for this kind of problems the amount of computational resources needed are far more expensive and time consuming than using the technique proposed here.

To arrive to this technique the GFSE's for the wave equation in Cartesian and cylindrical coordinates in one, two and three dimensions were found. Also, several GF for first and second kind boundary conditions were found to be used with their

corresponding GFSE. The GFSE is one and unique for a given geometry but the GF depends on the geometry and the boundary conditions.

Although the purpose of this work was to present a model for the Rijke tube, this technique can also be applied to any problem where the wave equation is considered, such as in MRI's, mufflers, and vibrations just to mention some examples. Also this technique can be applied in problems where 1-D variable speed of sound can be assumed. This feature allows accounting for the different fuel composition effects since the temperature profile is related to the fuel composition.

6.2. FUTURE WORKS

Experimental data obtained from different blends of fuel and air is needed to measure the scope of the technique proposed here. It is also proposed as a future work to break the results in two waves, one traveling upstream and the other downstream and introduce a reflection factor in order to gain accuracy in the theoretical results. Or by changing the reflection coefficient in the equations to make the results match the experimental values an accurate reflection coefficient could be determined.

This technique can be also used to solve problems in other fields of the engineering such as transient heat conduction.

REFERENCES

1. Warnatz, J., Maas, U., Dibble, R., "Combustion-Physical and Chemical Fundamentals, Modeling and Simulation, Experiments, Pollutant Information", 2nd Edition, Springer, Germany, 1999.

2. Lieuwen, T., Torres, H. Johnson, C. Zinn, B. T., "A Mechanism of Combustion Instability in Lean Premixed Gas Turbine Combustors", International Gas Turbine and Aeroengine Congress and Exhibition, ASME 99-GT-3, June, 1999.

3. Lieuwen, T., Zinn, B. T., "Theoretical Investigation of Combustion Instability Mechanisms in Lean Premixed Gas Turbines", 36th Aerospace Sciences Meeting and Exhibit, AIAA 98-0641, January, 1998.

4. Richards, G. A. and Robey, E.H. "Control of Flame Oscillations with Equivalence Ratio Modulation", Journal of Propulsion and Power, vol. 15, # 2, pp 232-240, 1999.

5. Blackshear, P. L., "Driving Standing Waves by Heat Addition", Fourth Symposium International on Combustion, pp 553-566, The Williams and Wilkins Co., Baltimore, 1952.

6. Dowling, A. P., "The Calculation of Thermoacustic Oscillations", Journal of Sound and Vibration, vol. 180, pp 557-581, 1995.

7. Crocco, L., Grey, J., Harrje, D. T., "Theory of Liquid Propellant Rocket Combustion Instability and Its Experimental Verification", American Rocket Society Journal, vol. 30, pp 159-168, 1960.

8. Culik, F. E. C., "A Note on Rayleigh's Criterion", Combustion Science and Technology, vol. 56, pp 159-166, 1987.

9. Neuringer, J. L. and Hudson, G. E., "An investigation of sound vibrations in a tube containing a heat source", Journal of the Acoustical Society of America, vol. 24, pp 667-674, Nov. 1952.

10. Brookes, S., Cant, R., Dupere, I., Dowling, A., "Computational Modeling of Self-Excited Combustion Instabilities", Transactions of the ASME, vol. 123, pp 322-326, 2001.

11. Chatterjee, P., Vandsburger, U., Saunders, W., Khanna, V., Baumann, W., "On the Spectral Characteristics of a Self-Excited Rijke Tubre Combustor-Numerical Simulation and Experimental Measurements", Journal of Sound and Vibration, vol. 283, pp. 573-588, 2005.

12. Majdalani, J., Entezam, B., Van Moorhen, W., "Full-Scale Numercial Model of a Rijke-Type Pulse Combustor", 7th AIAA/CEAS Aeroacoustics Conference, May 2001, Maastricht, The Netherlands.

13. Truffin, K., Poinsot, T., "Comparison and Extension of methods for Acoustic Identification of Burners", Journal of Combustion and Flame, vol. 142, pp. 388-400, 2005.

14. Natarajan, J., Nandula, S., Lieuwen, T., Seitzman, J., "Laminar Flame Speeds of Synthetic Gas Fuel mixtures", ASME Turbo Expo 2005: Power for Land, Sea and Air. Proceedings of GT2005-68917, Reno-Tahoe, Nevada, 2005.

15. Schefer, R. W., "Reduced Turbine Emissions Using Hydrogen-Enriched Fuels", Combustion Research Facility, Sandia National Laboratories, Progress Report, Livermore, California, 2001.

16. Zhang, Q., Noble, D. R., Meyers, A., Xu, K., Lieuwen, T., "Characterization of Fuel Composition Effects in H2/CO/CH4 Mixtures Upon Lean Blowout", Proceedings of ASME/IGTI Turbo Expo 2005. GT2005-68907, Reno-Tahoe, Nevada, 2005.

17. Richards, G. A., McMillian, M., Rogers, W., Gemmen, R., Cully, S. "Issues for Low Emission, Fuel-Flexible Power Systems", Progress in Energy and Combustion Science.

18. Beck J.V., Cole K.D., Haji A. and Litkouhi B. 1992. Heat Conduction Using Green's Functions. Hemisphere Publishing Corporation, New York, USA.

19. Carslaw H.S. and Jaeger J.C. 1959. Conduction of Heat in Solids. Oxford University Press, London, England, pg 353-386.

20. Jackson J.D. 1999. Classical Electrodynamics. John Wiley & Sons, Inc. New York, USA.

21. Morse P.M. and Feshbach H. 1953. Methods of Theoretical Physics. Vol I, McGraw-Hill Book Company, Inc., New York USA, pg 791-895.

22. Ozisik M.N. 1993. Heat Conduction. John Wiley & Sons, Inc. New York, USA, pg 214-251.

23. Venkataraman N.S.; Pérez E. and Delgado I. Temperature Distribution in Spacecraft Mounting Plates with Discrete Heat Generation Sources Due to Conductive Heat Transfer. Acta Astronautica, Vol. 53, Issue 3, pp. 173-183, August 2003.

24. Oyediran, A., Darling, D., Radhakrishnan, K., 31st. Joint Propulsion Conference and Exhibit, San Diego, California, 1995.

25. Khana, V., "A Study of the Dynamics of Laminar and Turbulent Fully and Partially Premixed Flames", Ph.D. Dissertation, Virginia Polytechnic Institute and State University, Virginia, 2001.

26. Putnam, A. A. and Dennis, W. R., "Study of Burner Oscillations of the Organ-Pipe Type", Transactions of the ASME, vol. 75, pp 15-28, 1953.

27. Putnam, A. A. and Dennis, W. R., "Burner Oscillations of the Gauze-Tone Type", Journal of the Acoustical Society of America, vol. 26, pp 716-725, 1954.

28. Putnam, A. A. and Dennis, W. R., "A Survey of Organ-Pipe Oscillations in Combustion Systems", Journal of the Acoustical Society of America, vol. 28, pp 246-259, 1956.

29. Putnam, A. A. Combustion-Driven Oscillations in Industry, American Elsevier Publishing, New York, NY, 1971.

30. Carrier, G. F., "The mechanics of the Rijke tube", Quarterly Applied Mathematics, vol. 12, pp 383-395, 1955.

31. Crocco, L., Mitchell, C. E., "Nonlinear Periodic Oscillations in Rocket Motors with Distributed Combustion", Combustion Science and Technology, vol. 1, pp 147-169, 1969.

32. Feldman, K. T., "Review of the Literature on Rijke Thermoacoustic Phenomena", Journal of Sound and Vibration, vol. 7, pp 83-89, 1968.

33. Raun, R. L., Beckstead, M.W., Finlinson, J. C. and Brooks, K. P., "A Review of Rijke Tubes, Rijke Burners and Related Devices", Progress in Energy and Combustion Science, vol. 19, pp 313-364, 1993.

34. Hedge, U. G., Reuter, D., Zinn, B. T., Daniel, B. R., "Fluid Mechanically Coupled Combustion-instabilities in Ramjet Combustors", AIAA-87-0216, 1987.

35. Culik, F. E. C., "Combustion Instabilities in Liquid-Fuelled Propulsion Systems- an Overview", AGARD-CP-450, 1988.

36. Mongia, R., Dibble, R., and Lovett, J., "Measurement of air-fuel ratio fluctuations caused by combustor driven oscillations", The International Gas Turbine and Aeroengine Congress: Stockholm, Sweden, ASME, (98-GT-502), June 1998.

37. Peracchio, A. A. and Proscia, W. M., "Nonlinear heat-release/acoustic model for thermoacoustic instability in lean premixed combustors", The International Gas Turbine and Aeroengine Congress: Stockholm, Sweden, ASME, (98-GT-502), June 1998.

38. Poinsot, T. J., Trouve, A. C., Veynate, D. P., Candel, S. M., and Esposito, E. J., "Vortex Driven Acoustically Coupled Combustion Intabilities", Journal of Fluid Mechanics, vol. 177, pp. 265-292, 1987.

39. Culik, F. E. C., "Dynamics of Combustion Systems: Fundamentals, Acoustics, and Control", California Institute of Technology, Course given at NASA John H. Glenn Research Center, September, 2001.

40. Lieuwen, T., "Combustion Driven Oscillations in Gas Turbines", Turbomachinery International, February, 2003.

41. Ibrahim, Z. M., Williams, F. A., and Buckley, S. G., "A Review of Previous Studies of Oscillatory Combustion in Gas Turbines", UCSD-CER-05-04, San Diego, California, June, 2005.

42. Candel, S. M., and Poinsot, T. J., "Interactions Between Acoustics and Combustion", Proceedings of the Institute of Acoustics, pp. 103-153, 1988.

43. Moliere, M., "Stationary Gas Turbines and Primary Energies: A Review of Fuel Influence on Energy and Combustion Performances", International Journal of Thermal Sciences, vol. 39, pp 141-172, 2000.

44. Nord, L. O., Andersen, H. G., "Influence of Variations in the Natural Gas Properties on the Combustion Process in Terms of Emissions and Pulsations for a Heavy-Duty Gas Turbine", ASME, Proceedings of International Power Generation Conference, Atlanta, Georgia, 2003.

45. Hendricks, A., Vandsburger, U., "The Effect of Fuel Composition on Flame Dynamics", Experimental Fluid and Thermal Science, Vol. 32, pp. 126-132, 2007.

46. Gaydon, D. E., "The Spectroscopy of Flames", 2nd edition, Chapman and Hall, London, 1974.

47. Diederichsen, J., and Gould, R. D., "Combustion Instability: Radiation from Premixed Flames of Variable Burning Velocity", Combustion and Flame, vol. 9, pp. 25-31, 1965.

48. Raffel, M., Willert C., Kompenhans J., "Particle Image Velocimetry", Springer, Germany, 1998.

49. Ferguson, D. H., "Experimental Investigation of Oscillatory Heat Release Mechanisms and Stability Margin Analysis in Lean-Premixed Combustion", PhD. Dissertation, West Virginia University, 2005.

50. Shao, W., Mechefske, C. K., "Acoustic Analysis of a Finite Cylindrical Duct Based on Green's Functions", Journal of Sound and Vibration, vol. 287, pp 979-988, 2005.

51. Greenberg M.D. 1971. Application of Green's Functions in Science and Engineering. Prentice-Hall Inc. Editors, New Jersey, USA.

52. Kreyszig, E., Advanced Engineering Mathematics, 8th edition, John Wiley and Sons Inc, 1998.

53. Wylie, R and Barret, L., "Advanced Engineering Mathematics", 6th edition. Mc Graw-Hill, 1995.

54. Sujith, R. I., Waldherr, G. A., Zinn, B. T., "An Exact Solution for One-Dimensional Acoustic Fields in Ducts with an Axial Temperature Gradient", Journal of Sound and Vibration, vol. 184, num.3, pp. 389-402.

APPENDICES

APPENDIX A

DIRAC-DELTA FUNCTION: Proof of second property

Consider $\int_{\alpha}^{\beta} f(x)\delta(x-\xi)dx$ where $\alpha < \xi < \beta$ as shown in figure A.1:

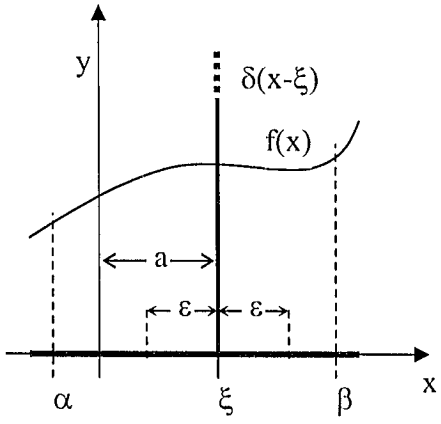

Where: $\varepsilon \to 0$

Fig. A.1. Integration of Dirac-delta

According to figure A.1 the integral can be broken up as follows:

$$\int_{\alpha}^{\beta} f(x)\delta(x-\xi)dx = \int_{\alpha}^{\xi-\varepsilon} f(x)\delta(x-\xi)dx + \int_{\xi-\varepsilon}^{\xi+\varepsilon} f(x)\delta(x-\xi)dx + \int_{\xi+\varepsilon}^{\beta} f(x)\delta(x-\xi)dx$$

Since $\delta(x-\xi) = 0$ if $x \neq \xi$, then the first and third terms on the right hand side vanishes, therefore:

$$\int_{\alpha}^{\beta} f(x)\delta(x-\xi)dx = 0 + f(\xi)\int_{\xi-\varepsilon}^{\xi+\varepsilon} \delta(x-\xi)dx = f(\xi)$$

Then: $\int_{\alpha}^{\beta} f(x)\delta(x-\xi)dx = f(\xi)$

APPENDIX B

DERIVATION OF THE GF FOR DIFFERENT COMBINATION OF BOUNDARY CONDITIONS

ONE-DIMENSIONAL GF

CASE I:

By applying orthogonality principles the values of the coefficients were found to be:

$$a_2 = \frac{2}{\omega L}\int_0^L g(x)\sin(kx)dx$$

$$b_2 = \frac{2}{L}\int_0^L h(x)\sin(kx)dx$$

And the final solution is:

$$p(x,t) = \int_0^L \frac{2}{\omega L}\sum_{n=1}^{\infty}\sin(kx)\sin(\omega t)\sin(kx')g(x')dx' + \int_0^L \frac{2}{L}\sum_{n=1}^{\infty}\sin(kx)\cos(\omega t)\sin(kx')h(x')dx' \qquad (B1)$$

When h(x) and g(x) are specified then the integration can be performed and the final solution can be found.

Recall the GFSE (11) to solve the same problem:

$$p(x,t) = \int_0^t \left\{\left(p\frac{\partial G}{\partial x'}\right)\Big|_0^{L} - \left(G\frac{\partial p}{\partial x'}\right)\Big|_0^{L}\right\}d\tau + \frac{1}{c^2}\int_0^L \left\{\left(p\frac{\partial G}{\partial \tau}\right)\Big|_{\tau=0} - \left(G\frac{\partial p}{\partial \tau}\right)\Big|_{\tau=0}\right\}dx' + \int_0^L\int_0^t GF d\tau dx'$$

The usual practice is, conveniently, to choose the boundary conditions for the auxiliary problem to be homogeneous and of the same kind of the boundary value problem to be solved. In this case $G(x,t|0,\tau) = G(x,t|L,\tau) = 0$

Since the boundary values are zero and there is no source, the GFSE is reduced to:

$$p(x,t) = \frac{1}{c^2}\int_0^L \left(\left(p\frac{\partial G}{\partial \tau}\right)\Big|_{\tau=0} - \left(G\frac{\partial p}{\partial \tau}\right)\Big|_{\tau=0} \right) dx'$$

But the initial conditions were given to be:

$p(x,0)=h(x)$; $p_t(x,0)=g(x)$

Then:

$$p(x,t) = \int_0^L \frac{1}{c^2} h(x)\left(\frac{\partial G}{\partial \tau}\right)\Big|_{\tau=0} dx' - \int_0^L \frac{1}{c^2} g(x) G\big|_{\tau=0} dx' \qquad \text{(B2)}$$

Equations (B1) and (B2) are the solution to the same problem using two different techniques; by comparing both results it can be easily noticed that:

$$G\big|_{\tau=0} = \frac{2c}{L}\sum_{n=1}^{\infty} \frac{1}{n\pi} \sin(kx)\sin(\omega t)\sin(kx')$$

Therefore:

$$\boxed{G = \sum_{n=1}^{\infty} \frac{2c}{n\pi} \sin(kx')\sin(kx)\sin(\omega[t-\tau])} \qquad \text{(B3)}$$

$$k = \frac{n\pi}{L} \quad \text{and} \quad \omega = kc \qquad \text{(B3.a)}$$

This last equation is the GF for the one-dimensional wave equation with Dirichlet boundary conditions.

Notice that the GF was found from the solution of the homogeneous case with homogeneous boundary conditions. These kinds of problems are relatively simple to solve. Then the GF can be applied to the GFSE to solve more complex problems.

Using a similarly procedure the problem with homogeneous boundary conditions can be solved and provide the GF. Next two more one-dimensional cases are presented.

CASE II

Boundary conditions of the second kind.

$$\left.\frac{\partial p}{\partial x}\right|_{x=0} = \left.\frac{\partial p}{\partial x}\right|_{x=L} = 0$$

And the respective GF is:

$$\boxed{G = \sum_{n=1}^{\infty} \frac{2c}{n\pi} \cos(kx') \cos(kx) \sin(\omega[t-\tau])} \qquad \text{(B4)}$$

With $k = \frac{n\pi}{L}$ and $\omega = kc$ (B4.a)

CASEIII

Dirichlet (or first kind) - Neumann (or second kind) boundary conditions.

$$\left.\frac{\partial p}{\partial x}\right|_{x=0} = p(L,t) = 0$$

And the GF is:

$$\boxed{G = \sum_{n=1}^{\infty} \frac{2c}{(2n+1)\pi} \cos(kx') \cos(kx) \sin(\omega[t-\tau])} \qquad \text{(B5)}$$

Where $k = \frac{(2n+1)}{2L}\pi$ and $\omega = kc$ (B5.a)

TWO-DIMENSIONAL GF

CARTESIAN COORDINATES

Although a variety of boundary conditions can be used and their respective GF be found; only three cases of interest for this study are presented next. Using equation (14) and the 2-D homogeneous version of the wave equation the GFs were found by using the same procedure as for the 1-D cases.

CASE I

Dirichlet boundary conditions at all the boundaries.

p(0,y,t) = p(L,y,t) = p(x,0,t) = p(x,H,t) = 0

H is the characteristic length in the y direction.

$$G = \sum_{n=1}^{\infty}\sum_{m=1}^{\infty}\frac{2c^2}{\omega LH}\sin(k_1 x')\sin(k_2 y')\sin(k_1 x)\sin(k_2 y)\sin(\omega[t-\tau])$$

$$\boxed{G = \frac{4c}{\pi LH}\sum_{n=1}^{\infty}\sum_{m=1}^{\infty}\frac{1}{\sqrt{\left(\frac{n}{L}\right)^2+\left(\frac{m}{H}\right)^2}}\sin(k_1 x')\sin(k_2 y')\sin(k_1 x)\sin(k_2 y)\sin(\omega[t-\tau])} \quad \text{(B6)}$$

Since $\omega = c\sqrt{k_1^2 + k_2^2}$ (B6.a)

$$k_1 = \frac{n\pi}{L} \quad \text{and} \quad k_2 = \frac{m\pi}{H} \quad \text{(B6.b)}$$

CASE II

Dirichlet boundary conditions on x and Neumann boundary conditions on y.

p(0,y,t) = p(L,y,t) = 0

$$\left.\frac{\partial p}{\partial y}\right|_{y=0} = \left.\frac{\partial p}{\partial y}\right|_{y=H} = 0$$

$$G = \sum_{n=1}^{\infty} \frac{2c}{n\pi H} \sin(k_1 x') \sin(k_1 x) \sin(k_1 ct) + \frac{4c}{\pi LH} \sum_{n=1}^{\infty} \sum_{m=1}^{\infty} \frac{\sin(k_1 x') \cos(k_2 y')}{\sqrt{\left(\frac{n}{L}\right)^2 + \left(\frac{m}{H}\right)^2}} \sin(k_1 x) \cos(k_2 y) \sin(\omega[t-\tau]) \quad \text{(B7)}$$

With $\omega = c\sqrt{k_1^2 + k_2^2}$ (B7.a)

$k_1 = \frac{n\pi}{L}$ and $k_2 = \frac{m\pi}{H}$ (B7.b)

CASE III

Boundary conditions as follows:

$$\left.\frac{\partial p}{\partial x}\right|_{x=0} = \left.\frac{\partial p}{\partial y}\right|_{y=0} = \left.\frac{\partial p}{\partial y}\right|_{y=H} = 0$$

p(L,y,t) = 0

And the GF is as follows:

$$G = \sum_{n=0}^{\infty} \frac{4c}{(2n+1)\pi H} \cos(k_1 x') \cos(k_1 x) \sin(k_1 c[t-\tau]) + \frac{4c}{\pi LH} \sum_{n=0}^{\infty} \sum_{m=1}^{\infty} \frac{\cos(k_1 x') \cos(k_2 y')}{\sqrt{\left(\frac{2n+1}{2L}\right)^2 + \left(\frac{m}{H}\right)^2}} \cos(k_1 x) \cos(k_2 y) \sin(\omega[t-\tau]) \quad \text{(B8)}$$

With $\omega = c\sqrt{k_1^2 + k_2^2}$ (B8.a)

$k_1 = \frac{(2n+1)\pi}{2L}$ and $k_2 = \frac{m\pi}{H}$ (B8.b)

CYLINDRICAL COORDINATES

Two cases were considered for cylindrical coordinates.

CASE I

Boundary conditions as follows:

$p(0,r,t) = p(L,r,t) = 0$

$p(x,r_0,t) = 0$

$$G = \frac{4c}{L(r_0)^2}\sum_{n=0}^{\infty}\sum_{m=1}^{\infty}\frac{\sin(k_1 x')J_0(k_m r')}{[J_1(k_m r_0)]^2\cdot\sqrt{\left(\frac{n\pi}{L}\right)^2 + k_m{}^2}}\sin(k_1 x)J_0(k_m r)\sin(\omega[t-\tau]) \quad \text{(B9)}$$

With $\omega = c\sqrt{k_1^2 + k_m^2}$ (B9.a)

$k_1 = \frac{n\pi}{L}$ and k_m are the zeroes of the eigenfunction $J_0(k_m r_0)=0$ (B9.b)

CASE II

For the boundary conditions:

$p(0,r,t) = p(L,r,t) = 0$

$$\left.\frac{\partial p}{\partial r}\right|_{r=r_0} = 0$$

$$G = \frac{4c}{L..\pi.r_0{}^2}\sum_{n=1}^{\infty}\frac{\sin(k_1 x)}{n}\sin(k_1 x).\sin\left(\frac{n.\pi}{L}c[t-\tau]\right) + \frac{4c}{L.r_0{}^2}\sum_{n=1}^{\infty}\sum_{m=1}^{\infty}\frac{\sin(k_1 x')J_0(k_m r')}{[J_0(k_m r_0)]^2\cdot\sqrt{\left(\frac{n\pi}{L}\right)^2 + k_m{}^2}}\sin(k_1 x)J_0(k_m r)\sin(\omega[t-\tau]) \quad \text{(B10)}$$

Notice that the first term comes from the fact that m=0 is also an eigenvalue making k_m=0 and the norm (i.e. the value of the integral in the denominator $\int_0^{r_0} r.J_0(k_m r)dr$) becomes $\int_0^{r_0} rdr = \frac{r_0^2}{2}$

With $\omega = c\sqrt{k_l^2 + k_m^2}$ (B10.a)

$k_l = \frac{n\pi}{L}$ and k_m are the zeroes of the eigenfunction $J_1(k_m r_0)$=0 (B10.b)

The eigenfunction for m=0 is $J_0(0)$=1

CASE III

For the boundary conditions:

$$\left.\frac{\partial p}{\partial x}\right|_{x=0} = 0$$

$$p(L,r,t) = 0 \quad \text{and} \quad \left.\frac{\partial p}{\partial r}\right|_{r=r_0} = 0$$

$$G = \frac{4c}{L(r_0)^2}\sum_{n=0}^{\infty}\sum_{m=1}^{\infty}\frac{\cos(k_l x')J_0(k_m r')}{[J_0(k_m r_0)]^2\sqrt{\left(\frac{(2n+1)\pi}{2L}\right)^2 + k_m^2}}\cos(k_l x)J_0(k_m r)\sin(\omega[t-\tau]) \quad \text{(B11)}$$

With $\omega = c\sqrt{k_l^2 + k_m^2}$ (B11.a)

$k_l = \frac{(2n+1)\pi}{2L}$ and k_m are the zeroes of the eigenfunction $J_1(k_m r_0)$=0 (B11.b)

CASE IV

With a similar approach followed in case II, it can also be obtained the 3-D GF after including the azimuthal variable (θ). The result is:

$$G=\sum_{n=1}^{\infty}\sum_{m=1}^{\infty}\sum_{\nu=0}^{\infty}\frac{2c}{\pi}\frac{\sin(\nu\theta').\sin(k_1 z').J_\nu(\lambda_m r')}{k.\left[\int_0^{r0} rJ_\nu(\lambda_m r)dr\right]^2}\sin(\nu\theta).\sin(k_1 z).J_\nu(\lambda_m r).\sin(k.c.[t-\tau]) \qquad \text{(B12)}$$

With

$$\omega = c.k \qquad \text{(B12.a)}$$

$$k=\sqrt{(k_1)^2+(\lambda_m)^2} \qquad \text{(B12.b)}$$

$k_1=\frac{n\pi}{L}$ and λ_m are the zeroes of the eigenfunction $J_\nu(\lambda_m r_0)=0$ (B12.c)